

## Original Study

## Open Access

Ajay Pratap Singh Rathor\*, Jitendra Kumar Sharma, Madhav Madhira

# An Analytical Study of Annular Raft on Granular Piles

<https://doi.org/10.2478/sgem-2024-0002>  
received July 15, 2023; accepted January 30, 2024.

**Abstract:** Rafts are frequently used to design foundations on soft soils to minimize the overall and differential settlements of structures built on them. In many cases, the raft alone can offer sufficient bearing capacity and all that is needed to restrict foundation settlements to a predetermined level with a few widely spaced piles. Granular piles (GPs) can be used due to their several advantages over steel or concrete piles. An annular raft foundation is generally provided for overhead water tanks, chimneys, etc. The provision of granular piles underneath the annular raft foundation not only increases the capacity of the foundation but also minimizes the settlement to an acceptable level. The present study deals with a rigorous analysis of annular raft foundation supported by GPs based on the continuum approach. A new numerical method is developed with geometric considerations for excluding the loaded pile portion from the region of the raft area by considering two distinct zones. This article introduces a novel approach, the annular raft over granular piles, which represents an innovative solution in geotechnical engineering. This innovation has the potential to improve the efficiency and effectiveness of foundation design in various construction projects. The response of annular raft foundation with GPs is evaluated in terms of settlement influence factor (SIF), load shared by granular piles (in %), and normalized shear stress variation along the GP–soil interface. The present study reveals that the presence of the pile influences the stress distribution locally. The stiffness of GP, relative length of GP, relative size of the raft influence the settlement and load sharing of annular raft with GPs.

**Keywords:** annular raft; granular pile; settlement influence factor; ring footing; shear stresses.

## 1 Introduction

The fundamental role of the foundation is to securely transfer the structure's load to the ground below with a minimal possible permissible settlement. Structures such as elevated water towers, chimneys, TV towers, and silos are typically built on annular rafts. The annular foundation is preferred because it suits the above structures and economics. In order to fulfill the requirements of full utilization of the bearing capacity of soil and for limited settlement, the annular raft is frequently the sole option in addition to being cost-effective. A rigorous analytical model for predicting the deformation of vertically loaded piles in granular soils using the elastic continuum approach was introduced [1]. Later, pile foundation analysis and design, including the elastic continuum approach for granular piles, were introduced [2]. The behavior of pile groups and piled rafts using the elastic continuum approach, focusing on the interaction between the piles and the surrounding soil, were investigated [3]. Adding piles underneath the raft provides additional strength to the foundation and reduces the settlement of the foundation. Granular piles are used extensively for ground improvement due to their low cost and better performance [4-11]. Comparing the combined piled raft foundation (CPRF) system with the pile foundation, it is possible to obtain the appropriate level of serviceability without compromising safety and performance [12]. Due to its affordability and better performance, various researchers have analyzed the performance and behavior of CPRF under the action of static as well as dynamic loading [13-18]. The different design approaches for CPRF were proposed in various studies [19-21]. The interaction analysis of two granular piled raft units was studied, and the influence of each GPR on another GPR was evaluated [22].

The elastic continuum approach is a fundamental framework used in geotechnical engineering to analyze

\*Corresponding author: **Ajay Pratap Singh Rathor**, Civil Engineering Dept., Rajasthan Technical University, University Department, Kota-324010, India, E-mail: [apsrathor.phd19@rtu.ac.in](mailto:apsrathor.phd19@rtu.ac.in)  
**Jitendra Kumar Sharma**, Civil Engineering Dept., Rajasthan Technical University, University Department, Kota-324010, India  
**Madhav Madhira**, Civil Engineering Dept., Jawaharlal Nehru Technological University & I.I.T. Hyderabad 500072, India

the behavior of soils and rocks. It considers these materials continuous and elastic, allowing for applying solid mechanics principles to study their response to various loading conditions. The elastic continuum approach can be used to analyze and predict the deformation, settlement, stress distribution, and stability of soil and rock structures, such as foundations, retaining walls, slopes, and tunnels. The elastic continuum approach assumes soils and rocks as homogeneous and isotropic materials. This simplification assumes that they exhibit linear elastic behavior within specific stress and strain ranges. The approach considers the fundamental concepts of stress, strain, and deformation, considering material properties, boundary conditions, and external loads.

The approach facilitates the design and assessment of geotechnical systems, considering factors such as load-bearing capacity, settlement limitations, and the prevention of failure mechanisms. The elastic continuum analysis considers the pile and the surrounding soil as a continuous medium, allowing for the evaluation of stress distribution, settlement, and pile–soil interaction. The elastic continuum approach helps to understand the load transfer mechanisms in granular piles, including the mobilization of skin friction.

The analysis of granular piles and combined granular piled raft systems using the elastic continuum approach offer a comprehensive understanding of their behavior under various loading conditions. This approach considers the interaction between the structure, piles, raft, and the surrounding soil, allowing for the assessment of performance and the optimization of design parameters. The performance of annular raft is analyzed by various researchers who found that it depends on various factors such as type of loading, type of soil, and size of annular raft and soil [23-32]. The inner and outer diameters play a vital role in the design of an annular raft which ultimately affects the settlement of the annular raft [33-40]. Some experimental studies were also carried out in order to analyze the settlement behavior of ring footing [41].

This study explicitly considers the presence of granular piles as the supporting medium for the annular raft. Previous research studies focused on other types of pile foundations or alternative support systems. Granular piles in this analysis recognize their relevance and address the specific challenges associated with this type of foundation system. This research utilizes an elastic continuum approach to analyze the behavior of the annular raft. Unlike discrete element methods or other numerical techniques that may have been employed in previous studies, the elastic continuum approach treats the raft and the supporting medium as continuous bodies.

This approach allows for considering the soil–structure interaction and evaluating stresses, displacements, and settlements within the system. The present analysis reveals previously unexplored phenomena, such as load distribution patterns, settlement mechanisms, or the influence of different parameters on the raft’s performance.

Advantages of choosing granular piles over conventional piles include cost-effectiveness, as granular piles can often be more economical than steel or concrete piles due to their simpler and quicker installation. Additionally, the ease of installation is a notable benefit, especially in loose or sandy soils, as granular piles do not require heavy machinery or specialized equipment. Another advantage is settlement control, where granular piles contribute to managing settlement by improving the load-bearing capacity of the soil, particularly in loose or compressible soils. However, it is essential to acknowledge certain limitations in the study, such as the nonlinear nature of the soil considered as isotropic in the present analysis. Furthermore, the validity of the analysis is restricted to a circular raft.

The present investigation brings a new perspective to analyze the annular rafts with granular piles by employing a thorough assessment that subtracts the granular pile area from the annular raft. The findings of this research are showcased in the form of design charts, which are readily accessible to engineers. In order to ensure the applicability of the results across different raft sizes, the outcomes are presented in the form of nondimensional parameters.

This study aims to evaluate the following parameters governing the performance of annular raft with granular piles.

- Settlement Influence Factor (SIF),  $I_{agpr}$ : The settlement influence factor is a dimensionless parameter that expresses the ratio of the settlement of a foundation to the settlement of the surrounding soil. It is often denoted by the symbol SIF and is used to characterize the relative settlement behavior of a foundation system.
- Normalized shear stresses,  $\tau_i$ , along the GP–soil interface
- Load shared (percentage) by GPs –  $P_{gp}$
- The ratio of settlements of an annular raft with GPs to the annular raft without GPs –  $S_r$

## 2 Problem Definition and Analysis

GPs are compressible with a deformation modulus of  $E_{gp}$ . The soft soil is characterized by its deformation modulus,  $E_s$ , and Poisson's ratio,  $\nu_s$ . The modular ratio,  $K_{gp} = E_{gp} / E_s$ , i.e., the ratio of modulus of deformation of GP to that of the soil, is used to define the relative stiffness of the granular piles.

Figure 1 depicts an annular raft with an outer diameter, ' $d_{ro}$ ' and inner diameter, ' $d_{ri}$ ' supported by granular piles each of length ' $L$ ' and diameter ' $d$ '. Granular piles are installed around the centroidal axis of the annular raft. The load applied to the annular raft pile system is  $P$ . Granular piles are characterized by deformation modulus, ' $E_p$ ' and Poisson's ratio, ' $\nu_p$ '. The annular raft rests on soil having Poisson's ratio, ' $\nu_s$ ' and deformation modulus, ' $E_s$ '. The problem is not strictly axisymmetric due to the presence of a finite number of piles. The interaction stresses between the soil and the raft vary both in the radial and tangential directions. In order to simplify the analysis, the raft is subdivided into sectors, 'A' and 'B,' as depicted in Figure 2. The variations of raft stresses in the tangential direction, i.e., with ' $\theta$ ,' in each sector are ignored. The annular raft is discretized into the ' $k_r$ ' number of equal area annular rings (Figure 3), and the annular raft is subdivided into ' $k_t$ ' angular subdivisions. Nodes for satisfying compatibility of settlements in sector 'A' are taken along the center line except in the region of GP, where they are taken a minimal distance away (0.01 times the diameter of the granular pile) from the periphery of GP to avoid problems of singularity, as shown in Figure 3 (a). The nodes for calculating settlements in sector 'B' are taken along the center line. Figure 3 (a) and (b) shows the stresses acting on the annular raft foundation and the global and local coordinate systems used for the purpose of numerical integration.

GP is discretized into  $n$  cylindrical elements (Figure 3b), each of which is subject to a shear ( $\tau$ ) at the GP-soil interface and uniform normal stress on the base,  $p_b$ . By integrating Mindlin's equation [42, 43] for vertical displacement due to vertical force, the soil displacements are calculated at the mid-point of the periphery of each element.

In the present study, the annular raft on granular piles is analyzed by using the elastic continuum approach.

The present study is based on the following assumptions:

- Isotropic, homogeneous, and linearly elastic soil: The surrounding soil is assumed to possess isotropic, homogeneous, and linearly elastic properties. This

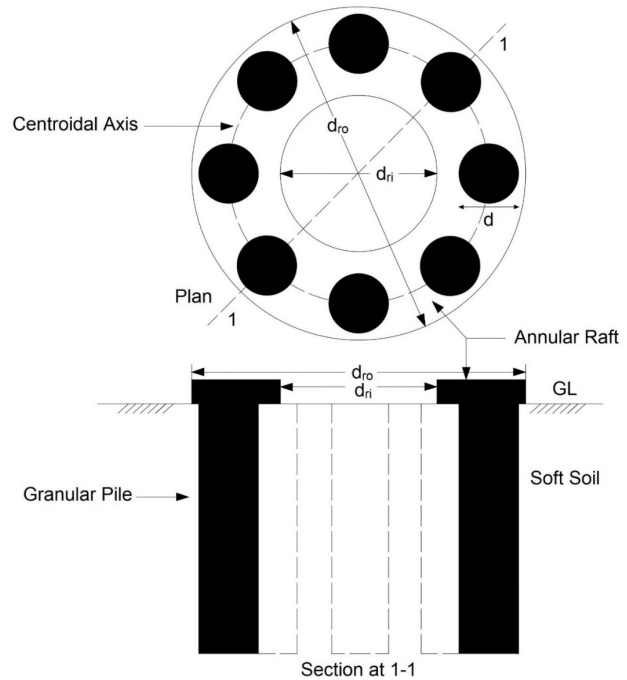


Figure 1: Schematic diagram of the annular raft over GPs.

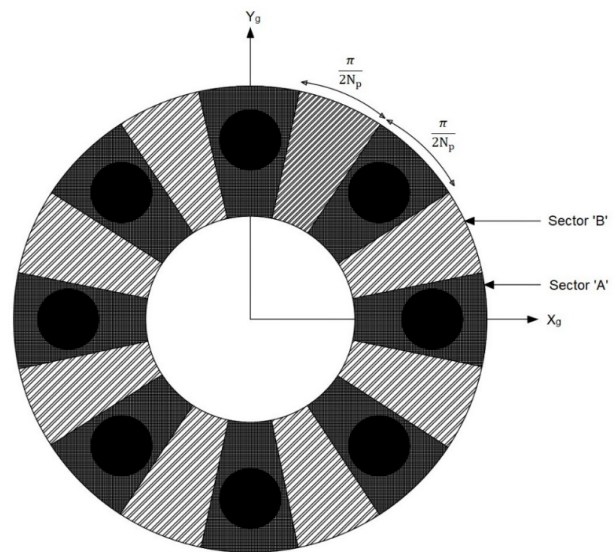


Figure 2: Annular raft subdivisions into sectors

simplifying assumption allows for easier analysis by considering uniform behavior in all directions.

- Perfectly rough sides of granular pile: The sides of the granular pile are assumed to have perfect roughness.
- Smooth and rigid granular pile base: The base of the granular pile is assumed to be smooth and rigid, enabling simplified calculations and analysis [43-44].

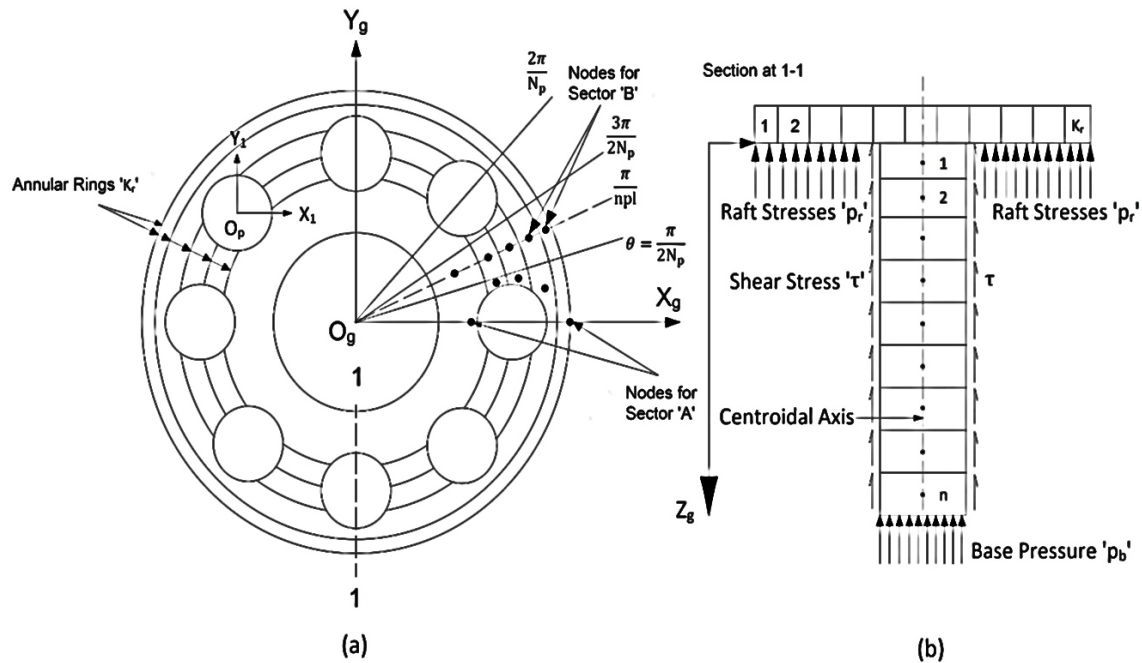


Figure 3: Discretization of (a) annular raft and (b) granular pile.

- Disregard of installation effects and consolidation: The effects of pile installation on the surrounding soil and the consolidation effects over time are neglected in this study.
- No slip or yield condition at the pile–soil interface: The pile–soil interface is assumed to have no slip or yield condition, simplifying the analysis of their interaction.
- Linear stress–strain relationship: The stress–strain pattern within the soil is assumed to be linear, following Hooke’s law.
- Rigid raft and uniform settlement: The raft is assumed to be rigid, and the surface beneath the raft is assumed to be smooth. Additionally, settlement is assumed to occur uniformly across the surface.

These assumptions provide a simplified framework for the analysis of the granular pile under specific conditions. However, it is essential to recognize that real-world conditions may deviate from these assumptions, and the results should be interpreted within the context of these simplifications.

### 3 Soil Displacements at the Nodes of Annular Raft

Soil displacements along annular raft are determined at the prescribed nodes of sectors ‘A’ and ‘B.’ For sectors ‘A,’ ‘B,’ and GP, the soil displacements are obtained due to the influence of stresses of sectors ‘A,’ ‘B,’ and GPs. Solutions for a point load in the interior and surface of a semi-infinite elastic continuum were provided in [45-47]. In order to obtain soil displacements due to the influence of stresses on sector ‘A,’ the influence area of the granular pile, which covers part of sector ‘A,’ is deducted. The geometric considerations for the deduction of GPs areas are explained in Fig. 4.

The condition for any annulus ‘j’ of an annular raft passing through the region of GP, as depicted in Figure 4, is

$$O_g V < r_o(j) < O_g U \quad \text{or} \quad O_g V < r_o(j-1) < O_g U$$

where  $r_o(j)$  and  $r_o(j-1)$  are the outer radii of annuli ‘j’ and ‘j-1,’ respectively. If any annulus ‘j’ is passing through the area of GPs, the condition for element ‘k<sub>i</sub>’ of annulus ‘j’ falling in the area of GP is to be investigated further. The central angle of any GP ‘l’ from the global axis,  $X_g$ , is

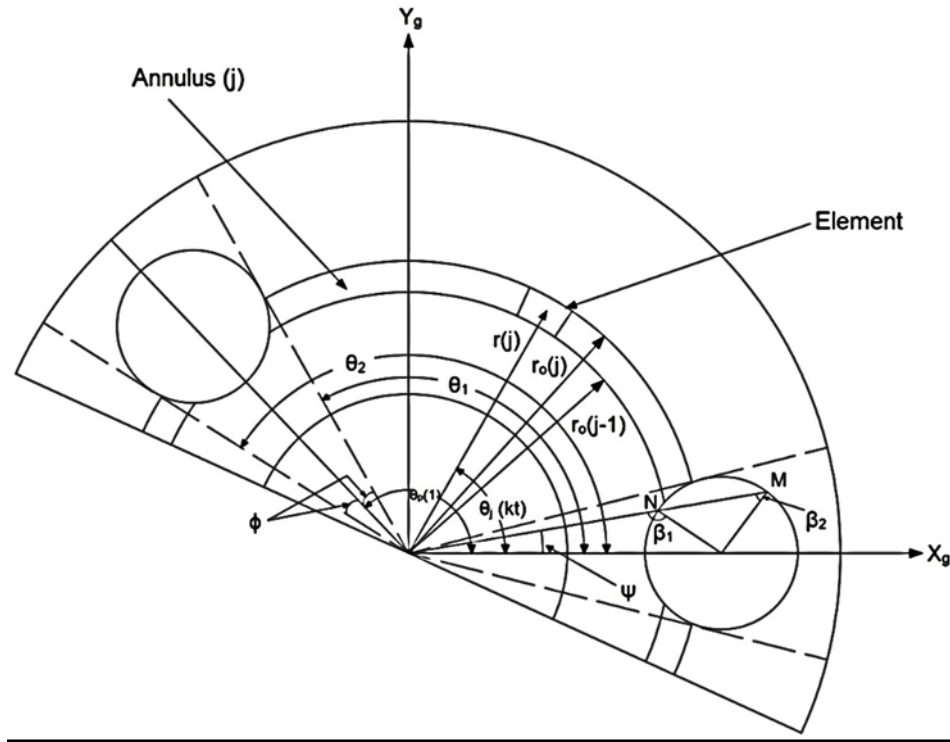


Figure 4: Geometrical consideration in integration scheme.

$$\theta_p(l) = \frac{2\pi}{N_p}(l - 1) \tag{1}$$

where 'l' varies from 1 to  $N_p$ . The angle 'phi' defined as the angle between the center line of any GP to its tangent, as shown in Fig. 4, is expressed as

$$\sin(\phi) = \frac{(d/2)}{O_g O_p} \tag{2}$$

where  $O_g O_p$  is the distance of the centroidal axis of the annular raft given as

$$2 \times O_g O_p = \left[ \frac{d_{ro}^2 + d_{ri}^2}{2} \right]^{1/2} \tag{3}$$

Angles of tangential lines of any GP 'l' are

$$\theta_1(l) = \theta_p(l) - \phi$$

$$\theta_2(l) = \theta_p(l) + \phi$$

The condition for element 'k<sub>t</sub>' of annulus 'j' falling in the granular pile region is  $\theta_1(l) < \theta_j(k_t) < \theta_2(l)$ , where  $\theta_j(k_t)$  is the angle element 'k<sub>t</sub>' of annulus 'j' that makes with global

axis,  $X_g$ . The elements near the GP periphery are further to be checked for their overlap. The essential condition of any element which fulfills the above condition and has its elemental angle  $\theta_j(k_t) = \psi$  with its centroidal distance  $r(j)$  is  $O_g N < r_0(j) < O_g M$ .

$O_g N$  and  $O_g M$  can be obtained from the property of triangle ( $\Delta O_g O_p N$  or  $\Delta O_g O_p M$ ) as

$$O_g N = \frac{(d/2)\sin(\beta_2 - \psi)}{\sin\psi} \tag{4}$$

$$O_g M = \frac{(d/2)\sin(\beta_2 + \psi)}{\sin\psi} \tag{5}$$

where  $\beta_2 = \sin^{-1}\left(\frac{2O_g O_p}{d} \sin\psi\right)$ . The soil displacement equations for sector 'A' of the annular raft are

$$\{\rho_A^{sa}\} = \left\{ \frac{S_A^{sa}}{d} \right\} = \left[ \sum_{l=1}^{l=N_p} [I_A^{sap}] \right] \left\{ \frac{\tau}{E_s} \right\} + [I_A^{saA}] \left\{ \frac{p_{rA}}{E_s} \right\} + [I_A^{saB}] \left\{ \frac{p_{rB}}{E_s} \right\} \tag{6}$$

where  $\{S_A^{sa}\}$  and  $\{\rho_A^{sa}\}$  are the soil displacement vector and normalized soil displacement vectors of size 'k<sub>r</sub>' each.  $[I_A^{sap}]$  is the influence coefficient matrix of soil displacement of size,  $k_r \times (n+1)$ , for the influences of interface shear stresses

and base pressure of any GP on nodes of sector 'A';  $[I_B^{saA}]$  is the influence coefficient matrix of soil displacement of size,  $k_r \times k_r$ , for nodes of sector 'A' and evaluated for the effect of contact stresses on sector 'A.'  $[I_B^{saB}]$  is the influence coefficient matrix of soil displacement of size,  $k_r \times k_r$ , for nodes of sector 'A' and evaluated for the effect of contact stresses on sector 'B.'  $\{P_{rA}\}$  and  $\{P_{rB}\}$  are the normal pressure column vectors of size,  $k_r$ , each for sectors 'A' and 'B,' respectively, and  $\{\tau\}$  is a column vector having size  $(n+1)$  for the shaft stresses and the normal stresses on the base of the pile.

For sector 'B' of the annular raft, the soil displacement equations are

$$\{\rho_B^{sa}\} = \left\{ \frac{S_B^{sa}}{d} \right\} = \left[ \sum_{l=1}^{l=Np} [I_B^{sal}] \right] \left\{ \frac{\tau}{E_s} \right\} + [I_B^{saA}] \left\{ \frac{p_{rA}}{E_s} \right\} + [I_B^{saB}] \left\{ \frac{p_{rB}}{E_s} \right\} \quad (7)$$

where  $\{S_B^{sa}\}$  and  $\{\rho_B^{sa}\}$  are the vectors of soil displacement and normalized soil displacement of sizes ' $k_r$ ' each for sector 'B.'  $[I_B^{sap}]$  is the influence coefficient matrix of soil displacement of size  $k_r \times (n+1)$  for the influences of interface shear stresses and base pressure of any GP on nodes of sector 'B';  $[I_B^{saA}]$  is the soil displacement influence coefficient matrix of size,  $k_r \times k_r$ , for nodes of sector 'B' and evaluated for the effect of contact stresses on sector 'A';  $[I_B^{saB}]$  is the soil displacement influence coefficient matrix of size,  $k_r \times k_r$ , for nodes of sector 'B' and evaluated for the effect of contact stresses on sector 'B.'

## 4 Granular Pile

In addition to the load, a granular pile's settlement is typically influenced by its geometry and deformation modulus. The magnitude of applied stress influences the granular material's deformation modulus. As a result, depending on the average principal stress at each level and the depth of the granular pile under loading, the deformation modulus may vary.

### 4.1 Granular pile displacement:

Displacement of the granular pile is evaluated by a generalized stress–strain relationship as

$$\varepsilon_{GP} = \frac{\sigma_{GP}}{E_{GP}} \quad (8)$$

where  $\varepsilon_{GP}$  is the axial strain of the element of granular pile and  $\sigma_{GP}$  is the axial stress on the element of granular pile.

### 4.2 Relationship between axial and shear stresses of GP:

In order to consider the equilibrium condition from Fig.4, the base pressure  $p_b$  and the shear stresses,  $\tau$ , are correlated with total load  $P$ , as

$$P = \sum_{j=1}^{j=n} \frac{\tau_j \pi d L}{n} + p_b \frac{\pi d^2}{4} \quad (9)$$

where  $n$  is the total number of elements of the granular pile.

The axial forces on the top and bottom face of an element 'i' are

$$P_{it} = P - \sum_{j=1}^{j=(i-1)} \frac{\tau_j \pi d L}{n} \quad (10)$$

$$P_{ib} = P - \sum_{j=1}^{j=i} \frac{\tau_j \pi d L}{n} \quad (11)$$

Combining equations (10) and (11)

$$P_{it} = \sum_{j=i}^{j=n} \frac{\tau_j \pi d L}{n} + p_b \frac{\pi d^2}{4} \quad (12)$$

$$P_{ib} = \sum_{j=(i+1)}^{j=n} \frac{\tau_j \pi d L}{n} + p_b \frac{\pi d^2}{4} \quad (13)$$

The axial stresses for the element 'i' on its top and bottom faces are

$$\sigma_{it} = p_b + \sum_{j=i}^{j=n} \frac{4(L/d)\tau_j}{n} \quad (14)$$

$$\sigma_{ib} = p_b + \sum_{j=(i+1)}^{j=n} \frac{4(L/d)\tau_j}{n} \quad (15)$$

The average axial stress on the element, 'i'

$$\sigma_{vi} = \frac{\sigma_{it} + \sigma_{ib}}{2} = p_b + \sum_{j=(i+1)}^{j=n} \frac{4(L/d)\tau_j}{n} + \frac{2(L/d)\tau_i}{n} \quad (16)$$

The relation between shear stresses and axial stresses of the element shown in the above equation can be expressed in the matrix form as

$$\{\sigma_v\} = [A_3]\{\tau\} \quad (17)$$

where  $\{\tau\}$  is the shear stress column vector of size  $(n+1)$  for the granular pile, including normalized stresses on the base, and  $\{\sigma_v\}$  is the axial stress column vector of size  $(n+1)$ .

Matrix  $[A_3]$  relates the shear and axial stresses as per equation (17), and it is an upper triangular matrix of size  $(n+1)$ .

$$[A_3] = \begin{bmatrix} \frac{2(L/d)}{n} & \frac{4(L/d)}{n} & \frac{4(L/d)}{n} & - & - & - & - & 1 \\ 0 & \frac{2(L/d)}{n} & \frac{4(L/d)}{n} & - & - & - & - & 1 \\ 0 & 0 & \frac{2(L/d)}{n} & - & - & - & - & 1 \\ - & - & - & - & - & - & - & - \\ - & - & - & - & - & - & - & - \\ - & - & - & - & - & - & - & - \\ - & - & - & - & - & \frac{2(L/d)}{n} & \frac{4(L/d)}{n} & 1 \\ - & - & - & - & - & 0 & \frac{2(L/d)}{n} & 1 \\ - & - & - & - & - & 0 & 0 & 1 \end{bmatrix} \quad (18)$$

### 4.3 Granular pile displacements:

The displacement of GP is determined from displacement of the top of the GP  $\rho_t$ . The settlement of the first element of the granular pile is

$$\rho_1^{ppv} = \frac{S_1^{ppv}}{d} = \rho_t - \varepsilon_{v1} \frac{\Delta z}{2d} \quad (19)$$

where  $\Delta z=L/n$  = the length of the element,  $\varepsilon_{v1}$  = the axial strain of GP's first element,

$S_1^{ppv}$  = the displacement of the first node, and  $\rho_1^{ppv}$  = the normalized displacement of the first node.

Thus, the displacement of any element 'i' is written as

$$\rho_i^{ppv} = \rho_t - \sum_{j=1}^{j=(i-1)} \varepsilon_{vj} \frac{\Delta z}{d} - \varepsilon_{vi} \frac{\Delta z}{2d} \quad (20)$$

where  $\varepsilon_{vi}$  is the axial strain of  $i^{\text{th}}$  element of GP and  $\varepsilon_{vj}$  is the axial strain of  $j^{\text{th}}$  element of GP.

In order to determine the settlement of the base of GP, the strain at the base is

$$\varepsilon_b = - \frac{dS^{ppv}}{dz} = \frac{p_b}{E_{gp}} \quad (21)$$

The above equation can be rewritten by using a finite difference scheme with unequal spacing intervals as

$$\frac{4S_{n-1}^{ppv} - 36S_n^{ppv} + 32S_{n+1}^{ppv}}{12(\Delta z/d)} = - \frac{p_b}{E_{gp}} \quad (22)$$

where  $S_{n-1}^{ppv}$  = displacement of element 'n-1',  $S_n^{ppv}$  = displacement of element 'n', and  $S_{n+1}^{ppv}$  = displacements of elements n+1.

The normalized form of the above equation is

$$4\rho_{n-1}^{ppv} - 36\rho_n^{ppv} + 32\rho_{n+1}^{ppv} = - \frac{p_b}{E_{gp}} \frac{12(L/d)}{n} \quad (23)$$

Substituting the values of  $\rho_{n-1}^{ppv}$  and  $\rho_n^{ppv}$  from Eq. (19) and rearranging the terms

$$\rho_{n+1}^{ppv} = \rho_t - \sum_{j=1}^{j=(n-2)} \varepsilon_{vj} \frac{\Delta z}{d} - \frac{34}{32} \varepsilon_{v(n-1)} \frac{\Delta z}{d} - \frac{18}{32} \varepsilon_{vn} \frac{\Delta z}{d} - \frac{6}{32} \frac{(L/d)p_b}{nK_{gp}E_s} \quad (24)$$

Combining equations (20) and (24) to get the vertical displacements of GP, one gets

$$\{\rho^{ppv}\} = \rho_t\{1\} + [B_3] \left\{ \frac{\sigma_v}{E_s} \right\} \quad (25)$$

where

$$[B_3] = \frac{(L/d)}{nK_{gp}} \begin{bmatrix} -0.5 & 0 & 0 & - & - & - & - & 0 \\ -1 & -0.5 & 0 & - & - & - & - & 0 \\ -1 & -1 & -0.5 & - & - & - & - & - \\ - & - & - & - & - & - & - & - \\ - & - & - & - & - & - & - & - \\ - & - & - & - & - & - & - & - \\ -1 & -1 & - & - & - & - & -0.5 & 0 \\ -1 & -1 & - & - & - & - & -\frac{34}{32} & -\frac{18}{32} & -\frac{6}{32} \end{bmatrix}_{(n+1) \times (n+1)} \quad (26)$$

Using the relationship between shear stresses and axial stresses (Eq. 17), the displacement of GP nodes in the vertical direction can be expressed in terms of shear stresses as

$$\{\rho^{ppv}\} = \rho_t\{1\} + [D_3] \left\{ \frac{\tau}{E_s} \right\} \quad (27)$$

where  $[D_3] = [B_3][A_3]$ , and the size of square matrix  $[D_3]$  is  $(n+1)$ .

#### 4.4 Soil displacement at the nodes of granular pile with annular raft:

Soil displacement equations for a granular pile are represented by Eq. 28,

$$\{\rho^{sp}\} = \left\{ \frac{S^{sp}}{d} \right\} = \left[ \sum_{l=1}^{l=Np} [I^{spvv}] \right] \left\{ \frac{\tau}{E_s} \right\} + [I^{spA}] \left\{ \frac{p_{rA}}{E_s} \right\} + [I^{spB}] \left\{ \frac{p_{rB}}{E_s} \right\} \quad (28)$$

where  $\{S^{sp}\}$  is the vector of soil displacements of size  $(n+1)$  and  $\{\rho^{sp}\}$  is the vector of normalized soil displacements of size  $(n+1)$  each for GP nodes.

$[I^{spvv}]$  is a square matrix of size  $(n+1)$  with the coefficients evaluated for the effect of elemental shear stresses and base pressure of the GP; the influence of stresses of all adjacent GPs is taken at the central nodes of GP as shown in Fig. 3 in order to achieve an average influence;  $[I^{spA}]$  is a matrix of size,  $(n+1) \times k_t$  with the coefficients evaluated for the effect of the contact stresses on sector 'A' on the GP node.  $[I^{spB}]$  is a matrix of size  $(n+1) \times k_t$  for the influence of contact stresses on sector 'B' on GP nodes.

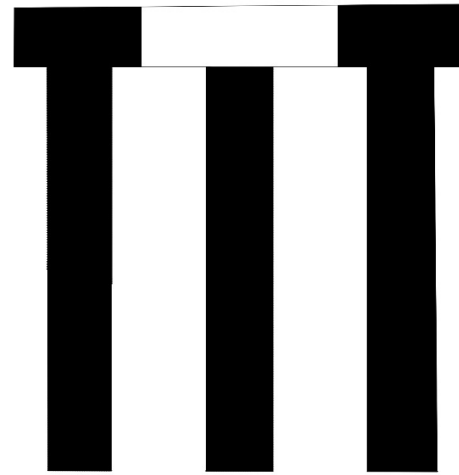
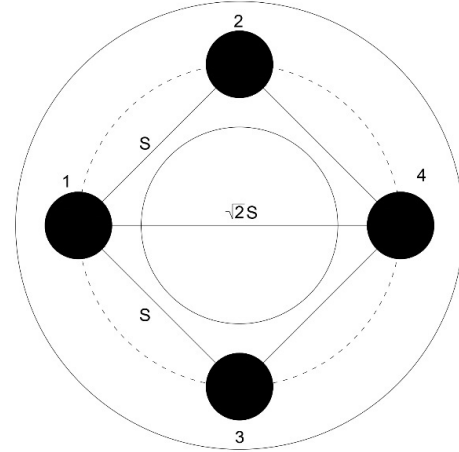


Figure5: Spacing of group of four GPs in terms of  $D_1$  and  $D_g$ .

### 5 Granular Pile and Annular Raft Displacements

The granular pile displacement equations are similar to equation (27)

$$\{\rho^{ppv}\} = \rho_t\{1\} + [D_3] \left\{ \frac{\tau}{E_s} \right\} \quad (29)$$

where  $[D_3]$  is a square matrix of size,  $(n+1) = [A][B]$ ,  $\{\rho^{ppv}\}$  is the normalized displacement vector of GP of size,  $(n+1)$ .  $\rho_t$  is the normalized top displacement of GP. The annular raft is considered rigid. Hence, the displacements of nodes of sectors 'A' and 'B' are all equal to the top displacement of GP,  $\rho_t$ . For sectors 'A' and 'B,' annular raft displacement equations are

$$\{\rho_A^{pa}\} = \rho_t\{1\} \quad (30)$$

$$\{\rho_B^{pa}\} = \rho_t\{1\} \quad (31)$$

### 6 Compatibility of Displacements

Solutions are obtained in terms of contact pressures for sectors 'A' and 'B' and shear stresses through the compatibility of displacements. Applying the compatibility condition for displacements of nodes in sector 'A' (Eqs (6) and (30))

$$\{\rho_A^{sa}\} = \{\rho_A^{pa}\} \left[ \sum_{l=1}^{l=Np} [I_A^{sapv}] \right] \left\{ \frac{\tau}{E_s} \right\} + [I_A^{saA}] \left\{ \frac{p_{rA}}{E_s} \right\} + [I_A^{saB}] \left\{ \frac{p_{rB}}{E_s} \right\} = \rho_t\{1\} \quad (32)$$

Similarly, for nodes in Sector 'B,' from Eqs. (7) and (31)

$$\{\rho_B^{sa}\} = \{\rho_B^{pa}\} \left[ \sum_{l=1}^{l=Np} [I_B^{sapv}] \right] \left\{ \frac{\tau}{E_s} \right\} + [I_B^{saA}] \left\{ \frac{p_{rA}}{E_s} \right\} + [I_B^{saB}] \left\{ \frac{p_{rB}}{E_s} \right\} = \rho_t\{1\} \quad (33)$$

For nodes along the granular pile, the compatibility condition from (Eqs (28) and (29)) is

$$\{\rho^{sp}\} = \{\rho^{ppv}\} \quad (34)$$

$$[E] \left\{ \frac{\tau}{E_s} \right\} + [I^{spA}] \left\{ \frac{P_{rA}}{E_s} \right\} + [I^{spB}] \left\{ \frac{P_{rB}}{E_s} \right\} = \rho_t \{1\}$$

where  $[E] = [\sum_{l=1}^{l=Np} [I^{spvv}]] - [D_3]$  of size  $(n+1) \times (n+1)$

Equations (32), (33), and (34) are solved simultaneously to obtain the contact pressures for sectors 'A' and 'B' and interfacial shear stresses along GP with the base pressure. The displacement of the annular raft is obtained from the evaluated stresses.

The settlement of the GP-annular raft foundation is expressed as

$$S_{agpr} = \frac{P}{E_s d} I_{agpr} \quad (35)$$

$$S_{ar} = \frac{P}{E_s d_o} I_{ar} \quad (36)$$

where  $I_{agpr}$  is the settlement influence factor for the annular raft on granular piles, which depends on the geometric and stiffness parameters related to GP and annular raft. The geometric parameters – annular ratio,  $D_r$ , and normalized annular width,  $D_g$ , related to annular raft dimensions – are defined as

$$D_r = \frac{d_{ri}}{d_{ro}}, \quad \text{where } 0 < D_r < 1 \quad \text{and} \quad (37)$$

$$D_g = \frac{d_{ro} - d_{ri}}{2d} \quad (38)$$

where  $d_{ro}$  and  $d_{ri}$  are the outer and inner diameters of the annular raft and 'd' is the diameter of the granular pile.  $S_{ar}$  is the normalized settlement of an annular raft only (without GPs), and  $I_{ar}$  is the SIF of an annular raft without GPs.

## 7 Spacing of Gps in Terms of $D_r$ and $D_g$

The spacing of a group of four granular piles is calculated in terms of  $D_r$  and  $D_g$  as follows. The granular piles are installed in such a way that the center of the GP lies on the equal area axis of the annular raft ( $r$ ). From Fig. (5), equal area of the annular raft can be written as

$$\pi(r^2 - r_i^2) = \pi(r_o^2 - r^2) \quad (39)$$

$$2r^2 = r_o^2 + r_i^2 \quad (40)$$

$$r = \sqrt{\frac{r_o^2 + r_i^2}{2}}$$

$$\sqrt{2}S = 2r \quad (41)$$

By substituting the value of r from equation (37), spacing S can be written as

$$S = \sqrt{2} \cdot \sqrt{\frac{r_o^2 + r_i^2}{2}} \quad (42)$$

By normalizing spacing with dia. of the pile (d), the above equation can be written as

$$\frac{S}{d} = \sqrt{\frac{d_{ro}^2 + d_{ri}^2}{4}} \quad (43)$$

Annular ratio ( $D_r$ ) and normalized annular width ( $D_g$ ) are defined as

$$D_r = \frac{d_{ri}}{d_{ro}} \quad \& \quad D_g = \frac{d_{ro} - d_{ri}}{2d} \quad (44)$$

$$d_{ri} = d_{ro} \cdot D_r$$

**Table 1:** Parameters used in the study.

S. No.	Parameters	Corresponding values
1.	$K_{gp}$	10–400
2.	$D_r$	0.2, 0.4, 0.6, 0.8
3.	$D_g$	2, 3, 4, 5
4.	L/d	5–40
5.	$N_p$	2–12

**Table 2:** Validation of the SIF values.

S.No.	Variable verified ( $D_r$ )	0.2	0.4	0.6	0.8
1.	Al Sanad (1993) [49]	0.814	0.709	0.532	0.345
2.	Egorov (1965) [50]	0.79	0.80	0.82	0.90
3.	Present analysis	0.80	0.80	0.81	0.85

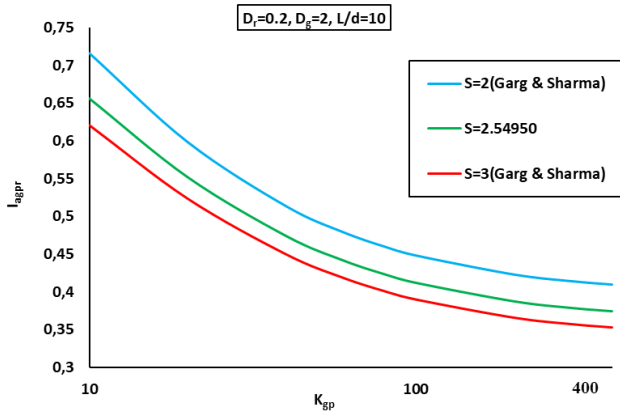


Figure 6: Comparison of variation of SIF with  $K_{gp}$  for different spacing [45].

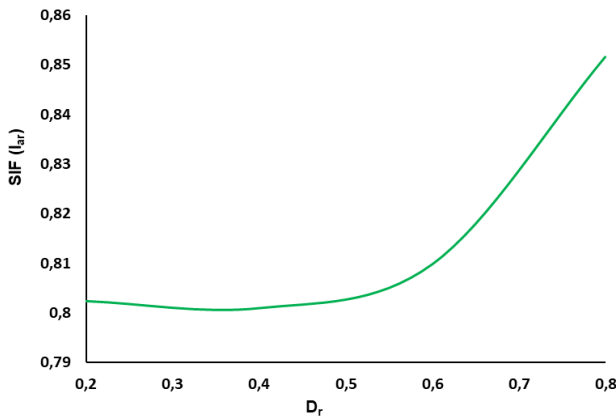


Figure 7: Variation of SIF (only annular raft without GPs) with  $D_r$ .

By substituting the value of  $d_{ii}$

$$D_g = \frac{d_{ro}(1-D_r)}{2d} \quad (45)$$

Now,  $d_{ro}$  and  $d_{ii}$  can be written as

$$d_{ro} = \frac{2dD_g}{1-D_r} \quad (46)$$

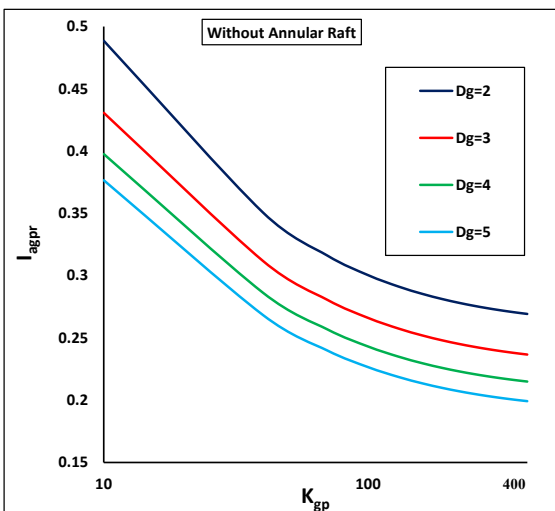
$$d_{ri} = \frac{2dD_g}{1-D_r} D_r \quad (47)$$

By substituting the values of  $d_{ro}$  and  $d_{ii}$  from equations (46) and (47) in equation (43), normalized spacing can be written as

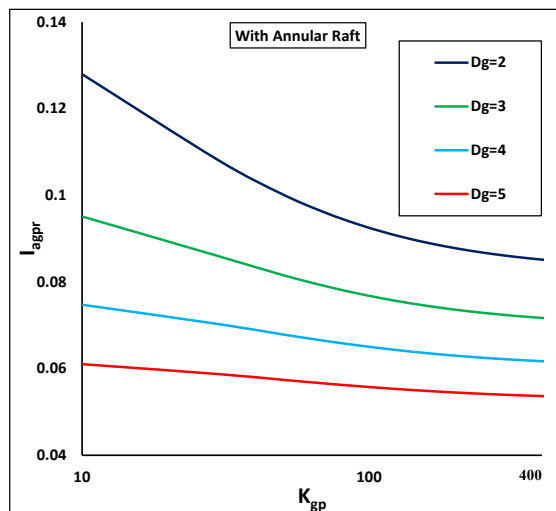
$$\frac{S}{d} = \sqrt{\frac{4d^2D_g^2}{(1-D_r)^2} + \frac{4d^2D_g^2}{(1-D_r)^2} D_r^2} \quad (48)$$

$$\frac{S}{d} = \sqrt{\frac{d^2D_g^2 + d^2D_g^2D_r^2}{(1-D_r)^2}}$$

The overall response of the GP–annular raft foundation is evaluated in terms of the settlement influence factor, the normalized GP–soil interfacial shear stresses, the percentage load carried by GP, and normal contact pressure distributions for sectors ‘A’ and ‘B’ of the annular raft. The parameters which affect the overall response of annular raft with GPs are (i) the geometric ones – the annular ratio,  $D_r$ , and normalized annular width,  $D_g$ , and length to diameter ratio of GP,  $L/d$ ; (ii) the number of



(a)



(b)

Figure 8: Variation of  $I_{agpr}$  with  $K_{gp}$  for a group of four GPs having  $D_r=0.2$  and  $L/d=10$  (a) without the annular raft and (b) with the annular raft.

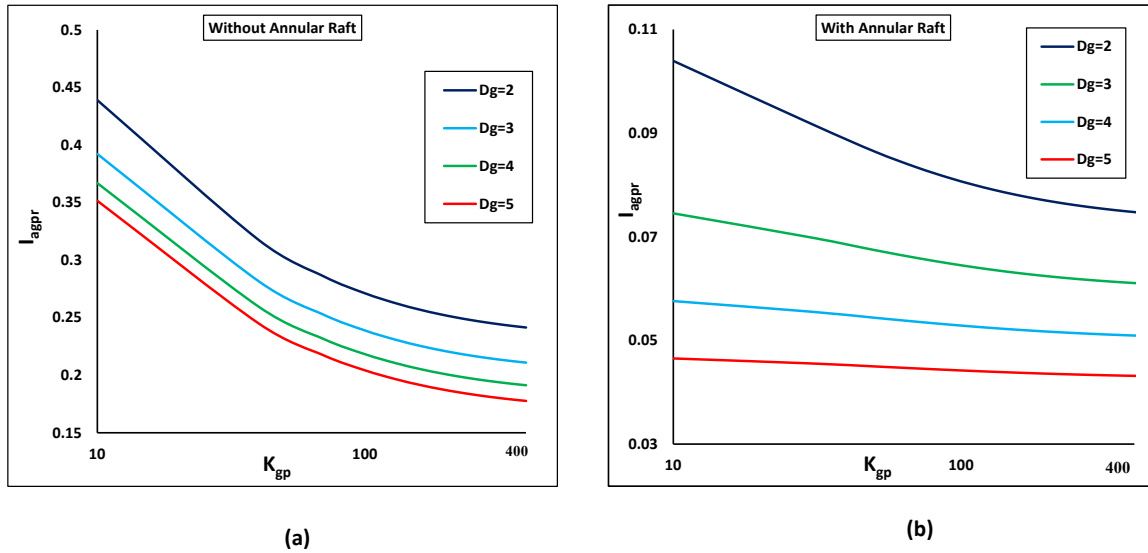


Figure 9: Variation of  $I_{agpr}$  with  $K_{gp}$  of the group of four GPs with and without raft for  $D_r=0.4$  and  $L/d=10$ : (a) without annular raft and (b) with annular raft.

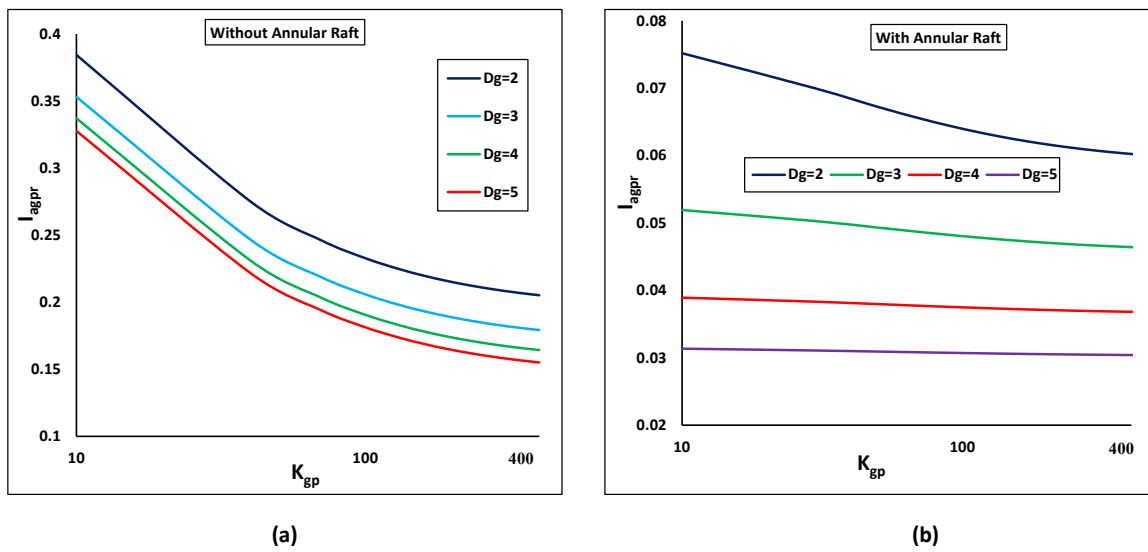


Figure 10: Variation of  $I_{agpr}$  with  $K_{gp}$  of a group of four GPs with and without raft for  $D_r=0.6$  and  $L/d=10$ : (a) without annular raft and (b) with annular raft.

granular piles,  $N_p$ ; and (iii) the relative GP–soil stiffness,  $K_{gp} = (E_p/E_s)$ .

## 8 Results and Discussion

### 8.1 Comparison of the present work

The results from the present study are validated with the previous one by [48] for a group of four GPs for spacings 2

and 3. Using the above expression of spacing, the spacing of four GPs is calculated in terms of  $D_r$  and  $D_g$ . The spacing achieved for  $D_r=0.2$  and  $D_g=2$  is 2.55, which lies in between the spacings 2 and 3.

As a result, a plot of SIF v/s  $K_{gp}$  is depicted in order to validate and compare the results, and with the spacing of 2.55, the SIF results are projected to fall between the spacings 2 and 3. The comparison of the present study is depicted in Fig. 6.

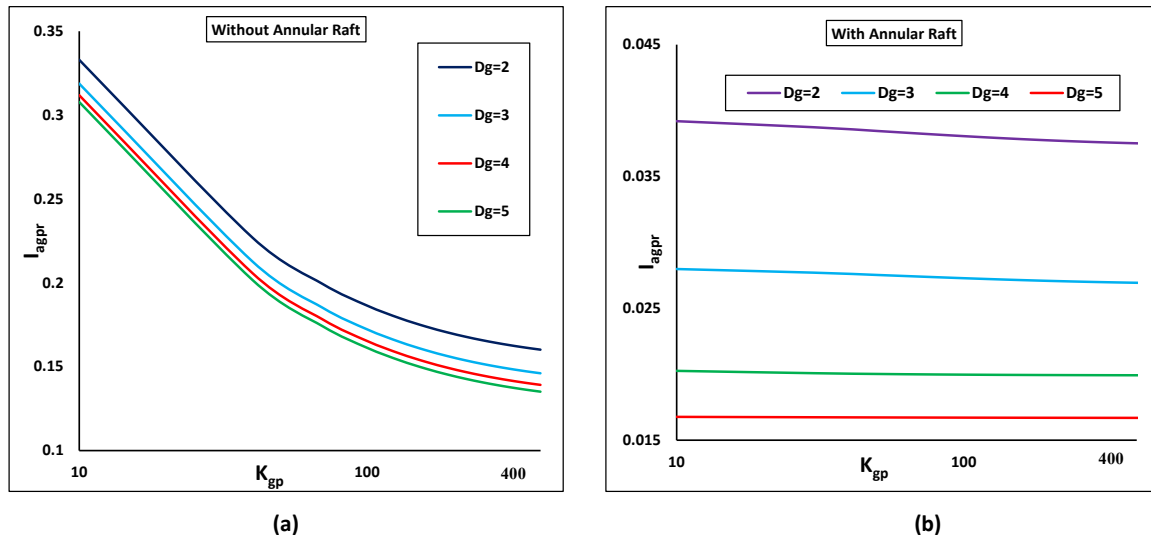


**Figure 11:** Variation of  $I_{agpr}$  with  $K_{gp}$  of a group of four GPs with and without raft for  $D_r=0.8$  and  $L/d=10$ .

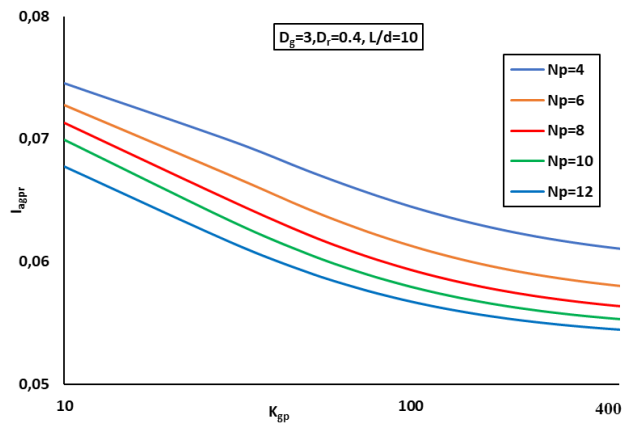


**Figure 12:** Variation of  $I_{agpr}$  with  $K_{gp}$  - Effect of number of granular piles ( $N_p$ ).

## 8.2 Validation of the present work

The SIF values of the present work are compared with the experimental work [41] that is shown in Table 2. The SIF values show good agreement with the experimental analysis of the annular raft conducted by [49-50].

Figure 7 can be referred to as a design chart to calculate the settlement of the annular raft. According to the results, increasing the annular ratio ( $D_r$ ) increases the value of the settlement influence factor ( $I_r$ ). The corresponding values of  $I_r$  for  $D_r=0.2$  and  $D_r=0.8$  are 0.8024 and 0.8010, respectively. It is observed that there is no significant change in the value of  $I_{ar}$  for  $D_r$  up to 0.6, and for  $D_r>0.6$ , the  $I_{ar}$  values significantly increased. As per the results, as the inner diameter of the annular raft

increases, the value of settlement of the annular raft also increases. The settlement of the annular raft increases as the inner diameter of the raft becomes larger. This is because, with a larger inner diameter, the annular raft behaves more like a strip, resulting in a reduced area of the raft. Consequently, the reduced area contributes to an increase in the settlement of the annular raft.

## 8.3 Parametric study:

The outcomes of a parametric investigation utilizing the continuum approach are disclosed, showcasing the solutions acquired across the specified parameter ranges detailed in Table 1.

The results of the above analysis are presented in the form of design charts for ready use. The effect of an annular raft resting on a group of GPs is evaluated by comparing the results of a group of four GPs with and without the annular raft. In the case of four GPs without the annular raft, the total load is equally distributed to the GPs, and the spacing of GPs is calculated in terms of  $D_r$  and  $D_g$  in order to keep the spacing of GPs same as GPs with the annular raft.

The variation of SIF ( $I_{agpr}$ ) with relative stiffness of GPs ( $K_{gp}$ ) is depicted in Figure 8 for normalized annular width ( $D_g$ ) range of 2–5,  $L/d=10$ , and annular ratio ( $D_r$ ) of 0.2. SIF for an annular raft with GPs is very less in comparison to SIF for GPs without a raft. It shows that the annular raft participates in the load transfer and significantly decreases the value of SIF. With the increase of the annular width, the area of the annular raft increases resulting in

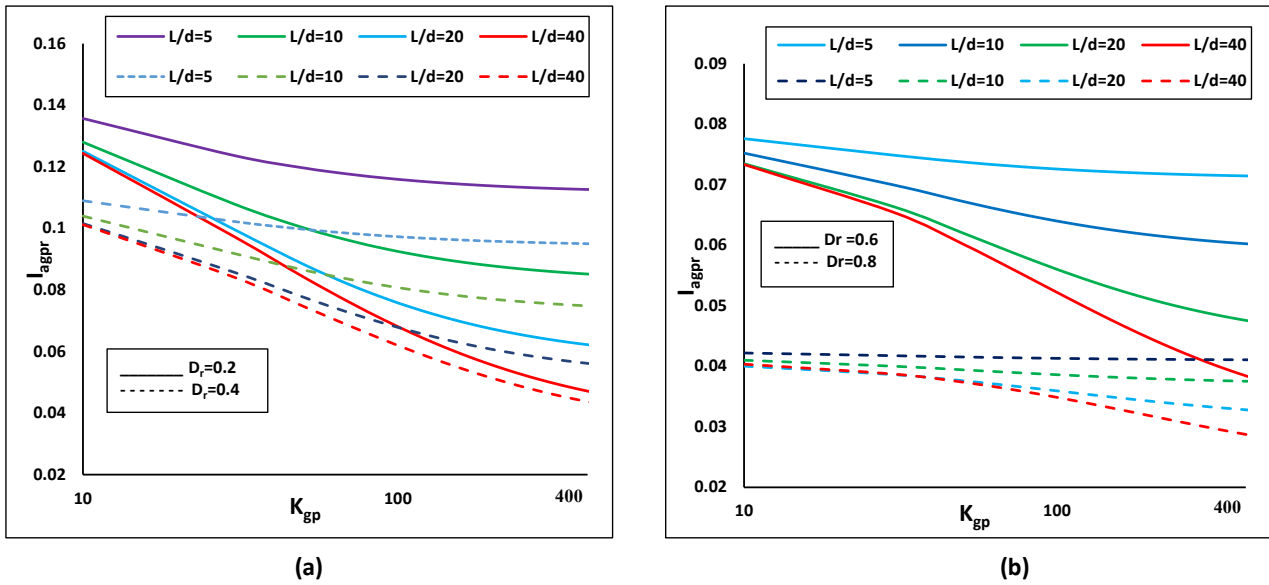


Figure 13: Variation of  $I_{agpr}$  with  $K_{gp}$  for  $D_g=2$ , with the effect of  $D_r$  and  $L/d$ : (a)  $D_r=0.2$  and  $0.4$  (b)  $D_r=0.6$  and  $D_r=0.8$ .

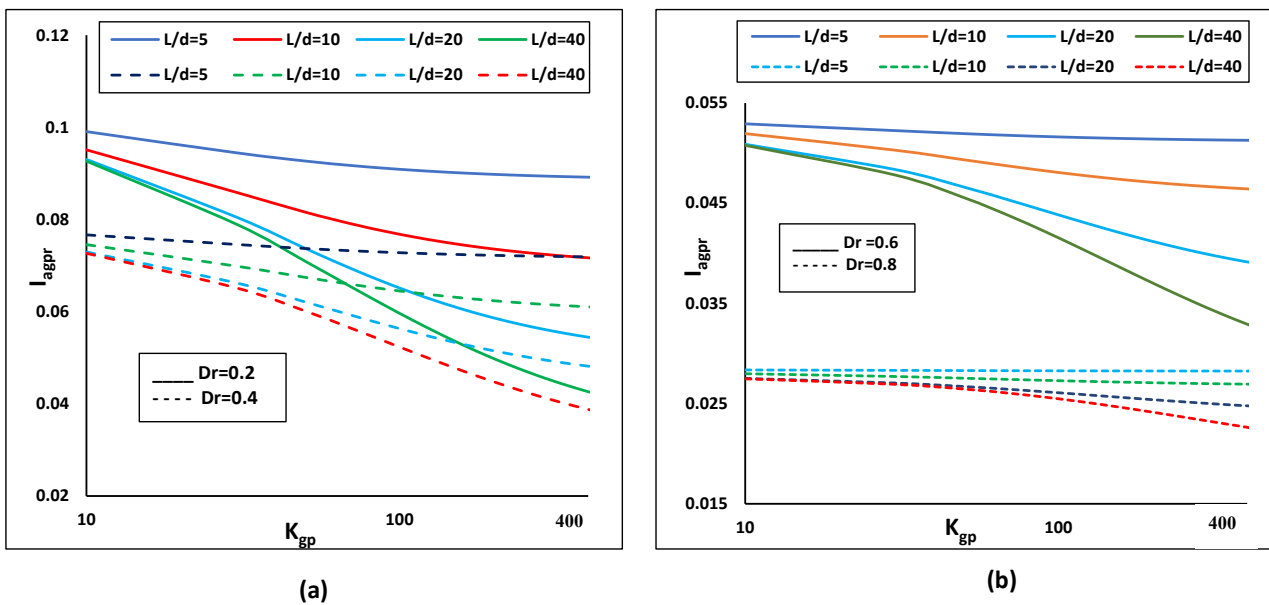


Figure 14: Variation of  $I_{agpr}$  with  $K_{gp}$  for  $D_g=3$  and with variation of  $D_r$  and  $L/d$ : (a)  $D_r=0.2$  and  $D_r=0.4$ ; (b)  $D_r=0.6$  and  $D_r=0.8$ .

smaller values of SIF. SIF for the annular raft with GPs decreases marginally with the increase of relative stiffness of GPs as expected.

The rate of decrease of SIF with  $K_{gp}$  decreases with the increase of  $D_g$ . A higher annular ratio,  $D_r$ , represents the higher internal diameter of the annular raft, i.e., a large area of the annular raft for the same value of annular width. Thus, the effect of granular piles in reducing the settlement influence factor of annular raft decreases with the increase of  $D_r$ .

SIF value for  $D_r = 0.2$  and  $D_g = 2$  decreased from 0.128 to 0.085 for  $K_{gp}$ , increasing from 10 to 400. Corresponding values for  $D_r = 0.2$  and  $D_g = 5$  are 0.061 and 0.054 for  $K_{gp} = 10$  and 400, respectively. The values of SIF are very high comparatively for four GPs without raft for the same spacing. It shows that the annular raft participates in load transfer and reduces the settlement.

For the parameters used in Figure 8, SIF is evaluated for  $D_r = 0.4$  and depicted in Figure 9. These results are very similar to those given in Figure 8.

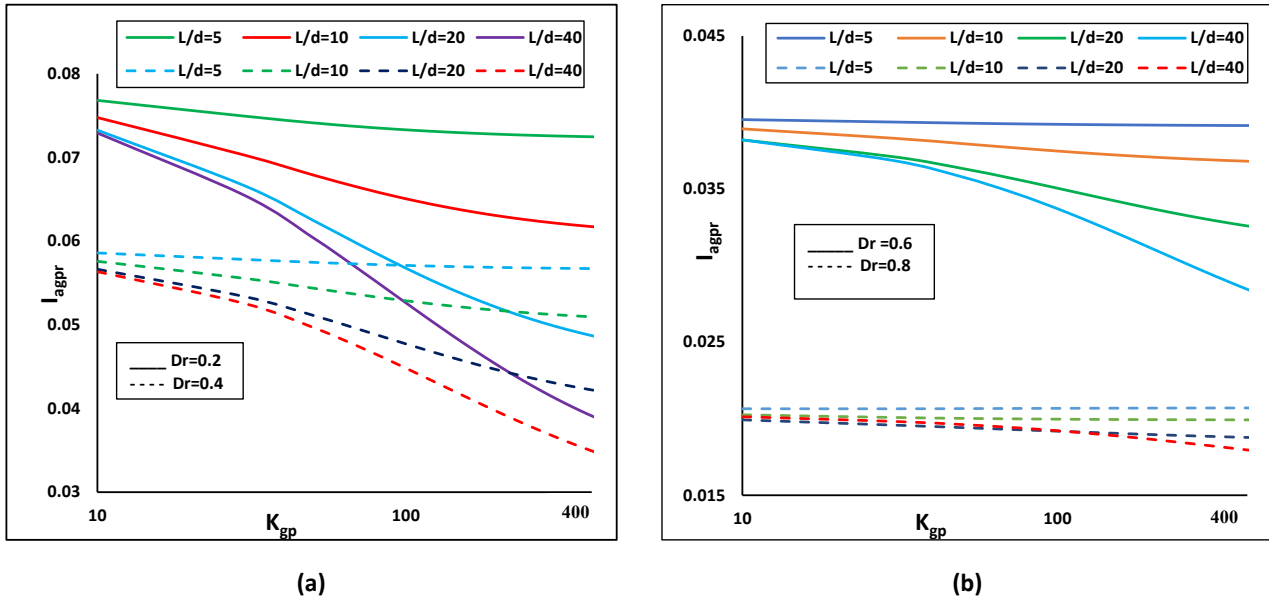


**Figure 15:** Variation of  $I_{agpr}$  with  $K_{gp}$  for  $D_g=4$  and with variation of  $D_r$  and  $L/d$ : (a)  $D_r=0.2$  and  $D_r=0.4$ ; (b)  $D_r=0.6$  and  $D_r=0.8$ .

SIF values for  $D_r=0.4$  and  $D_g=2$  are 0.104 and 0.074 for  $K_{gp}=10$  and 400, respectively. Corresponding values for  $D_r=0.4$  and  $D_g=5$  are 0.046 and 0.043 for  $K_{gp}=10$  and 400, respectively. SIF values decrease as expected with an increase in the annular ratio.

SIF values are evaluated for the same parameters as before, for  $D_r=0.6$ , it is depicted in Figure 10. The results are very similar once again to those shown in Figures 8 and 9. SIF values for  $D_r=0.6$  and  $D_g=2$  are 0.075 and 0.060 for  $K_{gp}=10$  and 400, respectively. Corresponding values for  $D_r=0.6$  and  $D_g=5$  are 0.031 and 0.030 for  $K_{gp}=10$  and 400, respectively. As the annular ratio increased from  $D_r=0.4$  to  $D_r=0.6$ , the SIF values decreased as expected, and the rate of decrease of SIF continuously decreased as the annular ratio increased.

Using the same parameters, SIF is evaluated for  $D_r=0.8$ , as depicted in Figure 11, and the results are very similar to those in Figures 8, 9, and 10. SIF values of  $D_r=0.8$  and  $D_g=2$  are 0.039 and 0.037 for  $K_{gp}=10$  and 400, respectively. Corresponding values for  $D_r=0.8$  and  $D_g=5$  are 0.017 and 0.016 for  $K_{gp}=10$  and 400, respectively. For a higher annular ratio, the spacing of GPs also increased, which results in lower values of SIF when only GPs are provided. The minimum rate of decrease of the SIF value is recorded for the highest annular ratio, i.e.,  $D_r=0.8$ . It shows that the annular raft significantly reduces the settlement when it is rested over a group of four granular piles.

For  $D_g$  values of 3 and 4, the  $I_{agpr}$  remains relatively constant. This can be attributed to the increased annular

width of the annular raft. With a wider annular width, the raft area increases, leading to a scenario where the majority of the load is borne by the annular raft rather than being shared by the granular piles (GPs). Consequently, the load on the GPs is reduced in these cases.

The variation of SIF with  $K_{gp}$  for different numbers of GPs for  $L/d=10$ ,  $D_r=0.4$ , and  $D_g=3$  is depicted in Figure 12. It is observed that by increasing the number of GPs, the SIF decreased as expected. The minimum value of SIF is recorded for 12 GPs. It is also observed that as the  $K_{gp}$  of GPs increases, the SIF also decreases. The significant change in the rate of change of SIF is up to the value of  $K_{gp}=100$ ; after that, the rate of decrease of SIF decreased.

In order to evaluate the effect of parameter  $L/d$  on SIF, the SIF variation with  $K_{gp}$  is depicted in Figure 13 (a) for  $D_g=2$ ,  $D_r=0.2$  and 0.4, and  $L/d=5-40$ . The comparison of SIF between  $D_r=0.2$  and 0.4 for a range of  $L/d$  is also shown in Figure 13 (a). The value of SIF for  $D_r=0.4$  is less than that of  $D_r=0.2$  for a particular  $L/d$  that shows the SIF decreases as the annular ratio increases. It is also observed from the above results that for larger  $L/d$ , the value of SIF decreases significantly up to the  $K_{gp}=100$ ; after that, the rate of decrease of SIF decreases. The rate of decrease of SIF is high up to  $K_{gp}=100$  due to the low-bearing capacity of the GPs, and the rate of decrease of SIF decreases after the value of  $K_{gp}=100$  because as  $K_{gp}$  increases, the load-bearing capacity of the GPs also increases.

The variation and comparison of SIF for  $D_r=0.6$  and 0.8 for different  $L/d$  are depicted in Figure 13 (b). It is observed from the results that for the same annular width

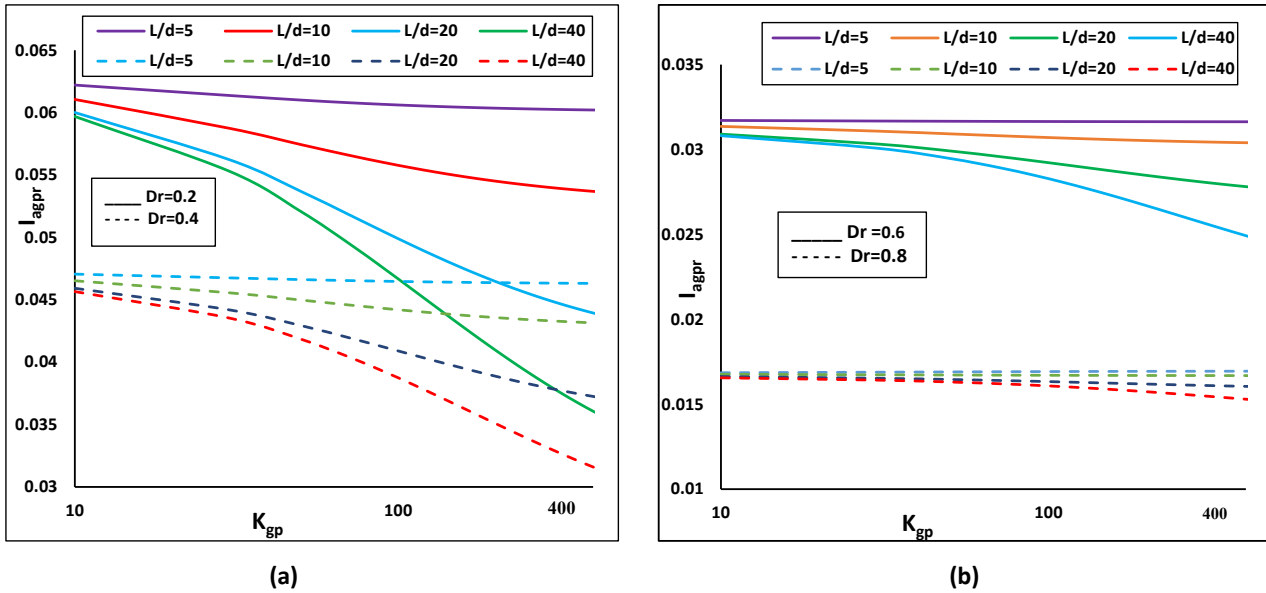


Figure 16: Variation of  $I_{agpr}$  with  $K_{gp}$  for  $D_g=5$  and with variation of  $D_r$  and  $L/d$ : (a)  $D_r=0.2$  and  $D_r=0.4$ ; (b)  $D_r=0.6$  and  $D_r=0.8$ .

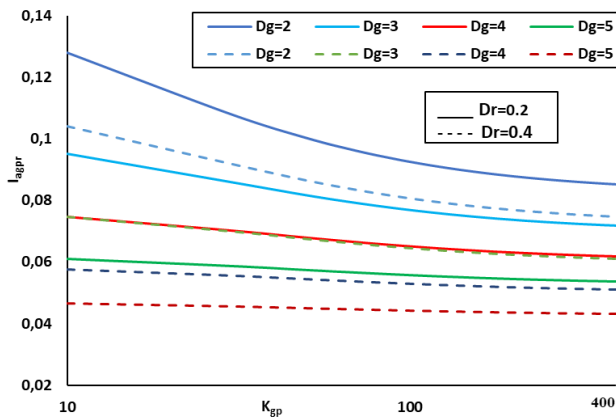


Figure 17: Variation of  $I_{agpr}$  with  $K_{gp}$ , effect of  $D_r$  and  $D_g$  for  $L/d=10$ .

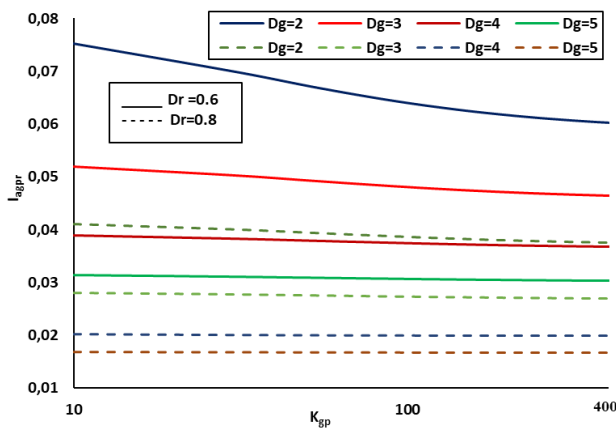


Figure 18: Variation of  $I_{agpr}$  with  $K_{gp}$ , effect of  $D_r$  and  $D_g$ .

( $D_g=2$ ) by increasing the annular ratio, the SIF decreases significantly, and the SIF values are also decreasing for GPs having a larger  $L/d$  ratio. As the relative stiffness of GPs ( $K_{gp}$ ) increases, the capacity of GPs increases; hence, SIF decreases. By increasing the annular ratio from 0.2 to 0.8 for  $D_g=2$  and  $L/d=5$ , the SIF value significantly decreased from 0.135 to 0.042 (i.e., 68.90% decrement). By increasing the  $L/d$  up to 40, for  $D_g=2$ , and  $K_{gp}=10$ , the SIF value for  $D_r=0.2$  and 0.8 decreased 67.54%, which shows that increasing the  $L/d$  of the GPs can reduce the settlement.

Similar results are obtained for  $D_g=3$ , for a range of  $D_r=0.2-0.4$  and  $L/d=5-40$  depicted in Figure 14 (a). The SIF value for  $D_g=3$ ,  $L/d=5$ , and  $K_{gp}$  decreases from 0.099 to 0.028 by increasing the  $D_r$  from 0.2 to 0.8.

The SIF values for  $D_g=3$  and  $L/d=5-40$  for greater  $D_r=0.6$  and 0.8 are evaluated and depicted in Figure 14 (b). It is observed from the results that the difference in SIF values in  $D_r=0.2$  to 0.4 is less in comparison to greater annular ratios, i.e.,  $D_r=0.6$  and 0.8. It is also observed that the SIF values are decreasing by increasing the annular width and  $L/d$ . For the same annular ratio and the annular width, increasing the  $L/d$  of GPs also significantly decreases the SIF values.

Similar results are obtained for  $D_g=4$ ,  $D_r=0.2-0.4$ , and  $D_r=0.6-0.8$  in Figure 15 (a) and (b), respectively. Similar trends and results are observed for the given range of parameters.

The SIF variation with  $K_{gp}$  is depicted in Figure 16 (a) for  $D_g=5$ ,  $D_r=0.2$  and 0.4, and different values of  $L/d$ .

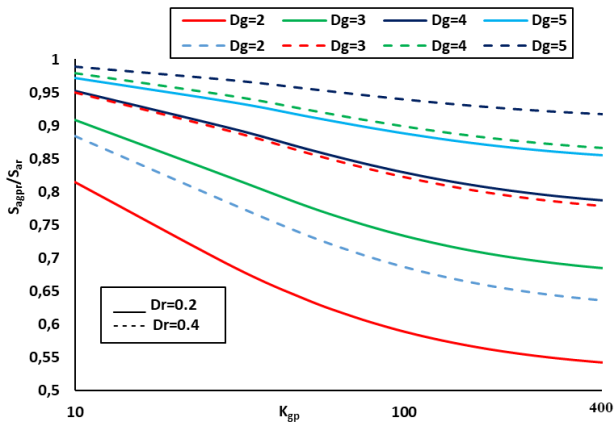


**Figure 19:** Variation of the ratio of settlement of annular granular piled raft to the settlement of annular raft,  $S_r$  with  $K_{gp}$  – effect of  $D_g$  for  $L/d=10$ .

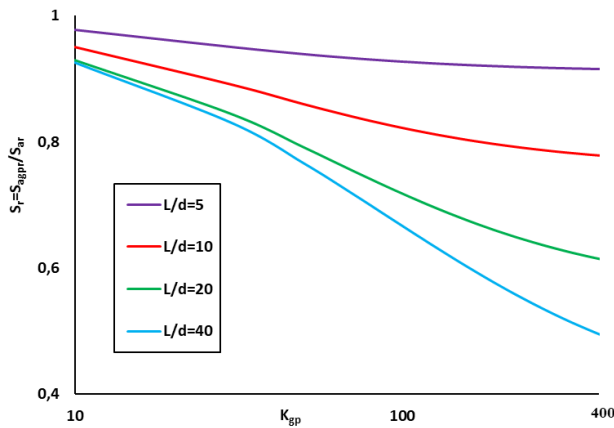


**Figure 20:** Variation of the ratio of settlement of annular granular piled raft to the settlement of annular raft,  $S_r$  with  $K_{gp}$  – effect of  $L/d$  for  $D_r=0.4$ ,  $D_g=3$ .

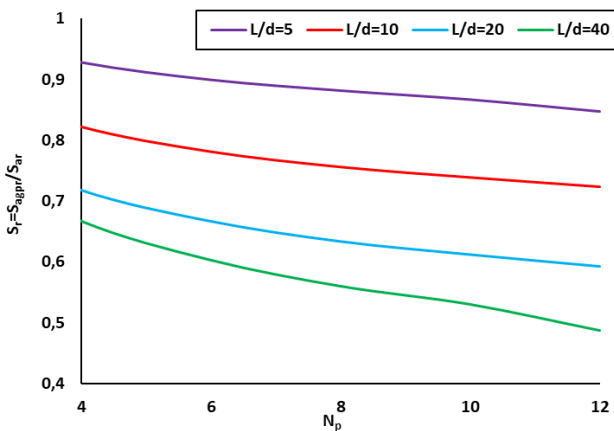


**Figure 21:** Variation of the ratio of settlement of the annular granular piled raft to the settlement of annular raft,  $S_r$  with  $N_p$  – effect of  $L/d$  for  $D_r=0.4$ ,  $D_g=3$ ,  $K_{gp}=100$ .

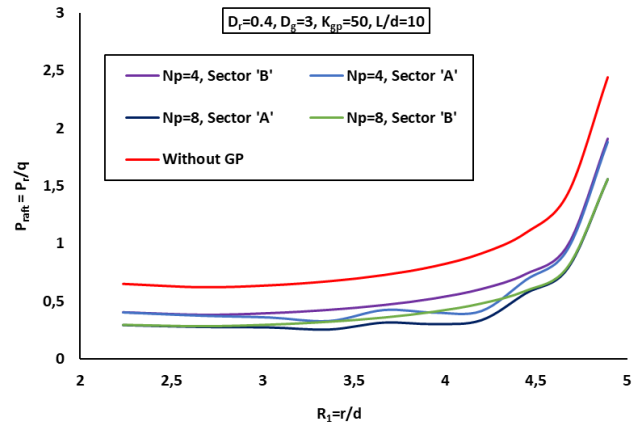


**Figure 22:** Variation of normalized contact pressure distribution at raft–soil interface,  $P_{raft}$  with normalized radial distance ( $R_r$ ) – effect of  $N_p$ .

It is observed that there is a significant decrement in SIF values for  $D_g=5$  in comparison to  $D_g=2$ . By increasing the  $D_g=2$  to  $D_g=5$ , by keeping  $D_r=0.2$ , and  $L/d=5$ , the SIF values for  $K_{gp}=10$  decreased up to 54.07%.

Similarly, the variation of SIF with  $K_{gp}$  for  $D_g=5$ ,  $D_r=0.6-0.8$ , and  $L/d=5-40$  is depicted in Figure 16 (b). For  $D_g=5$ , the comparison in SIF values between  $D_r=0.6$  and  $0.8$  for a range of  $L/d=5-40$  is comparatively more significant as compared to lower values of  $D_g$ . It is observed from the results that the rate of decrement of SIF values decreases by increasing  $D_r=0.6$  to  $0.8$ . The minimum SIF value is recorded for  $D_g=5$ ,  $D_r=0.8$ , and  $L/d=40$ .

In order to assess the effect of annular ratio and annular width simultaneously, the variation of SIF with  $K_{gp}$  is evaluated by keeping  $L/d=10$  for the group of four GPs.

The variation of SIF with  $K_{gp}$  is depicted in Figure 17 for  $D_r=0.2$  and  $0.4$  for the range of  $D_g=2-5$ . The results show that the SIF decreases significantly by increasing the annular ratio,  $D_r$ , and the annular width,  $D_g$ . As the relative stiffness of GPs ( $K_{gp}$ ) increases, the strength of the GPs increases; hence, the rate of decrease of SIF reduces. For the same annular ratio ( $D_r=0.2$ ), by increasing the annular width ( $D_g$ ) from 2 to 5, the SIF decreased 52.27%. Similarly, for the same annular ratio,  $D_r=0.4$ , by increasing the annular width ( $D_g$ ) from 2 to 5, the SIF decreased 55.24%. By providing an annular raft having  $D_r=0.4$ ,  $D_g=5$ , the SIF value decreased up to 63.63% as compared to an annular raft having  $D_r=0.2$ ,  $D_g=2$ . The results clearly show that the higher annular width has a comparatively larger area to distribute the load resulting in reduced values of SIF.

Similarly, the results are evaluated and depicted in Figure 18 for  $D_r=0.6$  and  $0.8$  and  $D_g=2-5$  for each  $D_r$ . The

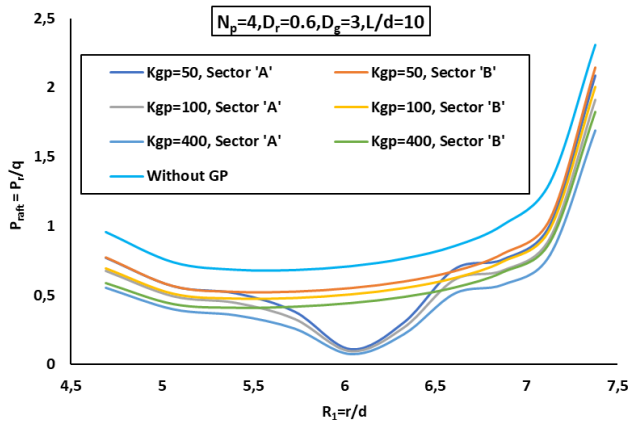


**Figure 23:** Variation of normalized contact pressure distribution at raft–soil interface,  $P_{raft}$ , with normalized radial distance ( $R_r$ ) – effect of  $K_{gp}$ .

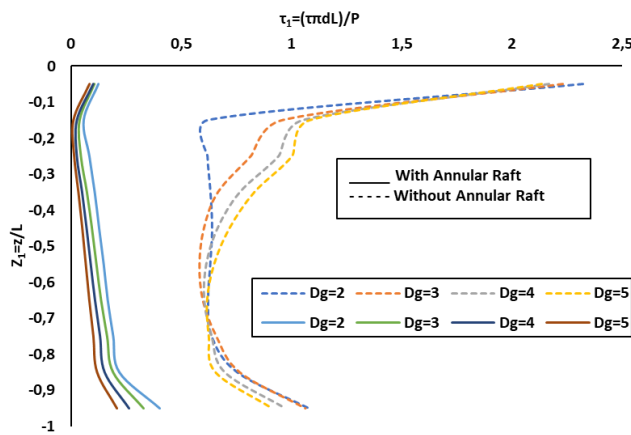


**Figure 24:** Comparison of normalized shear stress variation with the normalized depth for a group of four GPs with and without annular raft for  $D_r=0.2$ ,  $L/d=10$ , and  $K_{gp}=100$ .

SIF decreased for larger annular ratios, such as 0.6 and 0.8, and for the same annular ratio, and the SIF decreased by increasing the annular width due to the large size of the raft and the space between the GPs. For the same annular ratio ( $D_r=0.6$ ), by increasing the annular width ( $D_g$ ) from 2 to 5, the SIF decreased 58.29%. Similarly, for the same annular ratio,  $D_r=0.8$ , by increasing the annular width ( $D_g$ ) from 2 to 5, the SIF decreased 59.11%. By providing an annular raft having  $D_r=0.4$ ,  $D_g=5$ , the SIF value decreased up to 77.70% as compared to an annular raft having  $D_r=0.2$ ,  $D_g=2$ .

The variation of the ratio of settlements of the annular granular piled raft to the annular raft,  $S_{agpr}/S_{ar}$ , with  $K_{gp}$  is shown in Figure 19, along with the influence of  $D_g$ . The ratio of settlements decreases with the increase in the relative stiffness of GPs. The ratio,  $S_{agpr}/S_{ar}$ , is more for

larger values of  $D_g$  due to an increase in the area of the annular raft resulting in a reduction of the influence of GPs on settlement.  $S_{agpr}/S_{ar}$  values for  $L/d=10$ ,  $D_r=0.2$ , and  $D_g=2$  are 0.814 and 0.542 for  $K_{gp}=10$  and 400, respectively. Corresponding values for  $D_r=0.2$  and  $D_g=5$  are 0.972 and 0.854, respectively. Similar effects are observed with the increase of annular ratio,  $D_r$ .

The influence of the relative length of GPs is critically analyzed and depicted in the form of variation of the ratio  $S_{agpr}/S_{ar}$  with  $K_{gp}$  in Figure 20. The ratio of settlements decreases with the increase of  $L/d$ . The reductions are more for  $L/d$ , increasing from 10 to 20 in comparison to those for  $L/d$ , increasing from 20 to 40. The values of  $S_{agpr}/S_{ar}$  for  $K_{gp}=100$  is 0.817, 0.708, and 0.652 for  $L/d=10$ , 20, and 40, respectively. There is a 20.14% reduction in the value of the ratio  $S_{agpr}/S_{ar}$  by increasing the  $L/d=10$  to 40.

The variation of the ratio of the settlement of the annular granular piled raft to the settlement of the annular raft with  $N_p$  is depicted in Figure 21 for the evaluation of the effect of number of GPs. It is observed from the results that the value of  $S_r$  decreases by increasing the number of the pile ( $N_p$ ). It is also observed that by increasing the  $L/d$  of the GPs, the settlement ratio decreases by further increasing the number of GPs. By increasing the  $L/d$  of the GPs, the load-bearing capacity of the GPs increases, resulting reduction in the settlement ratio of the GPs. There is a significant reduction in the  $S_r$  by increasing  $L/d$ , and the rate of decrease increases as the  $L/d$  increases.

The normalized contact pressure distributions at the raft–soil interface ( $\beta_2 = \sin^{-1}(\frac{2D_g D_p}{d} \sin \psi)$ ) with normalized radial distance ( $R_r = r/d$ ) are depicted in Figure 22. For sectors ‘A’ and ‘B’ along with the influence of granular piles, the stresses for the sectors of the annular raft with GP, i.e., sector ‘A,’ are less particularly in the region close to the granular pile as compared to those for the sector without the granular pile, i.e., sector ‘B.’ The annular raft stresses at the inner and outer edges of the annular raft are almost identical for both sectors ‘A’ and ‘B’ of the annular raft. The raft stresses decrease with the increase of number of GPs. The value of  $P_{raft}$  at a radial distance of  $4d$  from the center of the annular raft without GP is 1.09 and decreased to 0.52, 0.45, and 0.40 for sector ‘B’ of the annular raft with number of GPs 4, 6, and 8, respectively.

Furthermore, the analysis reveals that increasing the number of granular piles (GPs) results in reduced stresses within the raft. This reduction occurs due to the load-sharing mechanism facilitated by the GPs.

The variation in stress distribution highlights an interesting observation: the contact stresses in sector A (the region where the piles are present) are lower compared to sector B. This disparity is primarily due

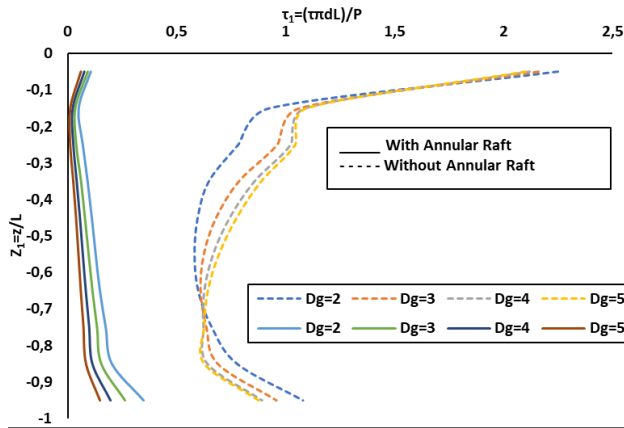


**Figure 25:** Comparison of normalized shear stress variation with the normalized depth for a group of four GPs with and without annular raft for  $D_r=0.4$ ,  $L/d=10$ , and  $K_{gp}=100$ .

to the presence of piles in sector A, which effectively redistributes and shares the load within that specific region. As a result, the raft experiences reduced contact stresses in the vicinity of the pile region (sector A) due to the load-bearing contribution of the GPs.

This observation underscores the significance of the presence of GPs in mitigating contact stresses and optimizing stress distribution within the raft system, particularly in the sector where the piles are located.

The annular raft stresses for sectors 'A' and 'B' decrease with the increase of relative stiffness of GPs, as presented in Figure 23. The reduction in stresses with  $K_{gp}$  is almost uniform along the radial distance from the inner edge of the annular raft to the outer edge of the annular raft. The contact stresses of the annular raft at the raft–soil interface are significantly reduced in the region of the pile in sector 'A.' It is observed that the raft contact stresses ( $P_{raft}$ ) are almost identical at the inner and outer edges of the annular raft for a particular  $K_{gp}$ , except in the region of the pile. As expected, the lowest value of raft stresses was recorded for the GP having  $K_{gp}=400$ .

The contact stresses at the interface between the annular raft and the underlying soil are significantly reduced in the region where the pile is located in sector 'A.' This reduction is attributed to the load-bearing contribution of the piles, which effectively redistributes and shares the load in that specific region.

The contact stresses ( $P_{raft}$ ) along the inner and outer edges of the annular raft are almost identical for a particular value of  $K_{gp}$ , except in the region of the pile. This observation aligns with expectations, as the presence of the pile influences the stress distribution locally.

The distribution of shear stresses along the GP–soil interface, normalized with the total load on an annular

raft, i.e.,  $[\tau_N = \tau / \pi d L]$  with a normalized depth of GP,  $Z_N = z / L$ , is depicted in Figure 24 for the influence of  $D_g$ .

The shear stress variation for a group of four granular piles is calculated with and without an annular raft in order to analyze the effect of the annular raft on the group of four GPs. The shear stresses decrease with the increase of  $D_g$  as the size of the raft increases. It is clear from the results that the annular raft plays a significant role in load bearing as compared to GPs. The shear stresses are significantly less in the GPs when the annular raft is provided over GPs. As the raft is placed over the GPs, the raft takes the maximum load, and the shear stresses induced at the GP–soil interface are less in the top portion of GPs and increased slightly near the base of the GPs.

For  $D_r=0.2$  and  $D_g=2$ , the value of shear stresses for a group of four GPs is recorded at 2.324, and for a Group of four GPs with an annular raft, the value of shear stress is 0.123 at the top of the GPs. It shows that by providing the annular raft, the shear stresses of the GPs are reduced up to 94% at the top of GPs and 72% at the base of the GPs. For  $D_g=3$ , the values of shear stresses for a group of four GPs with and without raft are recorded 0.107 and 2.233, respectively; at the top of the GPs and at the base of the GPs, the values are 0.329 and 1.064, respectively. For  $D_r=0.2$  and  $D_g=3$ , the shear stresses at the top of the GPs are reduced up to 95.20%, and at the base of the GPs, they are reduced up to 69.05%. Similarly, for  $D_g=5$ , the shear stresses of GPs with and without raft at the top of GPs are 2.134 and 0.084, respectively, and at the base of the GPs, they are 0.913 and 0.208, respectively. For  $D_g=5$ , the annular raft reduced the shear stresses of GPs up to 96.06% at the top of GPs and up to 77.22% at the base of the GPs. The results show that the annular raft significantly reduces the shear stresses of the GPs at the top and base of GPs.

The interfacial shear stresses in the group of four GPs with annular raft are calculated for the ranges of  $D_r=0.4$ , 0.6, and 0.8 also and compared with the shear stresses of a group of four GPs without annular raft at the same spacing as the spacing of GPs underneath the annular raft.

The shear stresses of a group of four GPs with and without annular raft for  $D_r=0.4$  are depicted in Figure 25. For  $D_r=0.4$  and  $D_g=2$ , the values of shear stresses for a group of four GPs with and without annular raft are recorded 0.106 and 2.248, respectively; at the top of the GPs and at the base of the GPs, they are 0.349 and 1.079, respectively. It shows that by providing the annular raft, the shear stresses of the GPs can be reduced up to 95.26% at the top of the GPs and 67.66% at the base of the GPs. By increasing the annular ratio from 0.2 to 0.4, the shear stresses of the GPs reduced 13.77% at the top of the GPs and 13.50% at the base of the GPs.

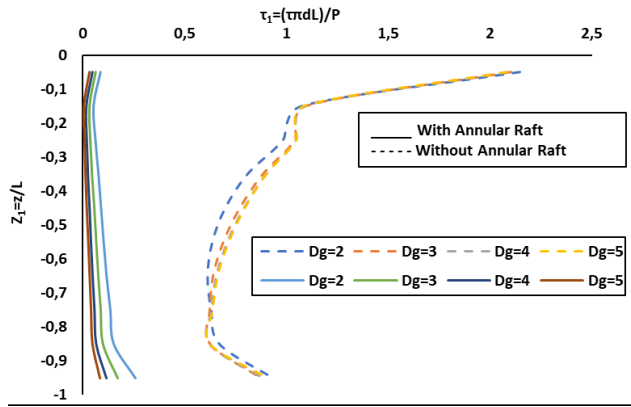


**Figure 26:** Comparison of normalized shear stress variation with the normalized depth for a group of four GPs with and without the annular raft for  $D_r=0.6$ ,  $L/d=10$ , and  $K_{gp}=100$ .

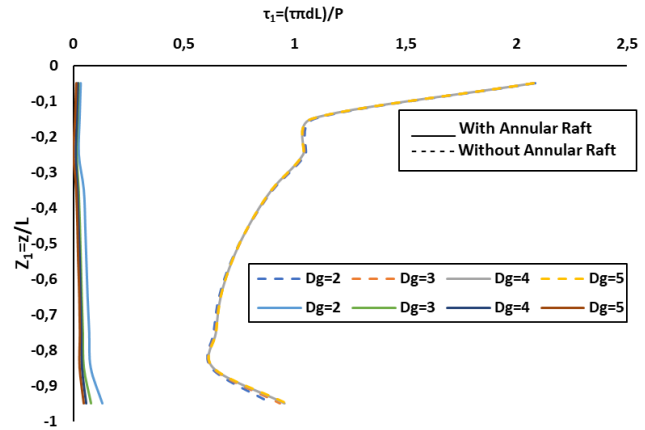


**Figure 27:** Comparison of normalized shear stress variation with the normalized depth for a group of four GPs with and without the annular raft for  $D_r=0.8$ ,  $L/d=10$ , and  $K_{gp}=100$ .

**Table 3:** Shear stresses and its reduction due to the presence of an annular raft.

$D_r$	$D_g$	Shear stresses of GPs without annular raft		Shear stresses of GPs with annular raft		Shear stresses reduction due to annular raft (%)	
		Top	Bottom	Top	Bottom	Top	Bottom
0.2	2	2.324458	1.079298	0.123507	0.403755	94.70	62.65
	3	2.232964	1.064219	0.107169	0.328567	95.20	69.17
	4	2.169796	0.974238	0.100482	0.263145	95.38	72.99
	5	2.134603	0.913877	0.084327	0.208937	96.06	77.21
0.4	2	2.248837	1.079708	0.106494	0.349187	95.28	67.66
	3	2.160045	0.957485	0.089982	0.261161	95.83	72.72
	4	2.120533	0.892764	0.074019	0.194048	96.51	78.26
	5	2.101452	0.876311	0.058483	0.145743	97.22	83.37
0.6	2	2.147183	0.935131	0.087404	0.259689	95.93	72.23
	3	2.103237	0.876795	0.063182	0.171468	97.00	80.44
	4	2.08833	0.886777	0.047783	0.11668	97.71	86.84
	5	2.082598	0.907918	0.03232	0.08452	98.45	90.69
0.8	2	2.085437	0.895009	0.033402	0.132094	98.40	85.24
	3	2.079723	0.934551	0.024073	0.080976	98.84	91.34
	4	2.079205	0.954441	0.020154	0.060053	99.03	93.71
	5	2.079428	0.963823	0.014868	0.047917	99.28	95.03

Similarly, by increasing the annular width  $D_g$  up to 5 for the same annular ratio,  $D_r=0.4$ , the shear stresses of the GPs further reduced due to the increased width of the annular raft. For  $D_r=0.4$  and  $D_g=5$ , the shear stresses of a group of four GPs with and without raft are recorded 0.058 and 2.101, respectively; at the top of the GPs and at the base of the GPs, they are 0.145 and 0.876, respectively.

By increasing the annular width of the annular raft, the shear stresses are reduced up to 97.21% at the top of the GPs and up to 83.36% at the base of the GPs as compared to only GPs.

Similar trends are obtained for  $D_r=0.6$  depicted in Figure 26. As the annular ratio  $D_r$  increased to 0.6, the shear stresses significantly reduced compared to smaller

annular ratios, i.e., 0.2 and 0.4. For  $D_r=0.6$  and  $D_g=2$ , the value of shear stresses for a group of four GPs with and without annular raft is recorded 0.087 and 2.147, respectively; at the top of the GPs and at the base of the GPs, they are 0.349 and 1.079, respectively. Similarly, the shear stresses reduced with the depth and slightly increased in the bottom portion of the GPs. As the annular width increased to 5 (i.e.,  $D_g=5$ ), the shear stresses of the GPs with and without raft decreased because of the increased size of the annular raft. The shear stresses for  $D_g=5$  for a group of four GPs with and without annular raft are recorded 0.032 and 2.083, respectively; at the top of the GPs and at the base of the GPs, they are 0.084 and 0.908, respectively. The shear stresses were reduced up to 98.44% at the top of the GPs and 90.69% at the base of the GPs.

The shear stress variation with depth for the annular ratio ( $D_r$ ) 0.8 for different annular width of the annular raft is depicted in Figure 27. The shear stresses for  $D_g=2$ , with and without a raft, are recorded 0.033 and 2.085, respectively; at the top of the GPs and at the base of the GPs, they are 0.132 and 0.895, respectively. By providing an annular raft over GPs, there is a reduction of shear stresses of GPs up to 98.39% at the top and 85.24% at the base of the GPs. By increasing the annular width up to  $D_g=5$ , the shear stresses of GPs with and without annular raft are recorded 0.014 and 2.079, respectively; at the top of the GPs and at the base of the GPs, they are 0.047 and 0.963, respectively. By increasing the annular width of the annular raft up to  $D_g=5$ , the shear stress of GPs reduced up to 99.28% at the top of the GPs and 95.03% at the base of the GPs.

It is seen from the above results that in comparison to only GPs, the annular raft over GPs can reduce the shear stresses of the GPs significantly and can transfer the maximum load. The annular raft reduces the shear stresses of GPs.

The annular ratio and the annular width play a significant role in the strength of the annular raft and its performance. As the annular ratio of the annular raft increased, the internal diameter of the annular raft increased, and the raft tended to behave like a strip, and the shear stresses of GPs got reduced. For a particular annular ratio, by increasing the annular width of the annular raft, a further significant reduction is seen in the shear stresses of GPs which proves the significance of the performance of the annular raft and cost reduction.

The shear stresses of GPs get reduced up to 13.77% at the top of the GPs and 13.35% at the base of the GPs while increasing the annular ratio from 0.2 to 0.4 for  $D_g=2$ .

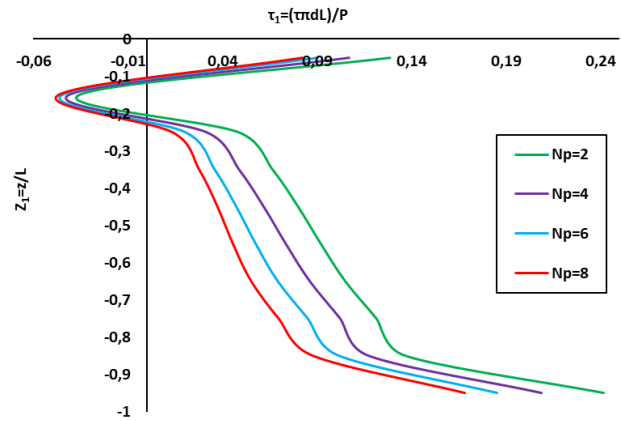


Figure 28: Variation of  $\tau_1$  with  $Z_1$  – effect of number of GPs for  $D_r=0.4$ ,  $D_g=3$ ,  $L/d=10$ , and  $K_{gp}=50$ .

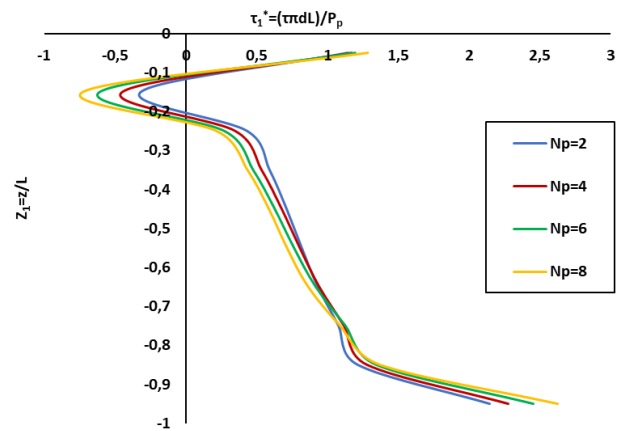


Figure 29: Variation of  $\tau_1^*$  with  $Z_1$  – effect of number of GPs for  $D_r=0.4$ ,  $D_g=3$ ,  $L/d=10$ ,  $K_{gp}=50$ .

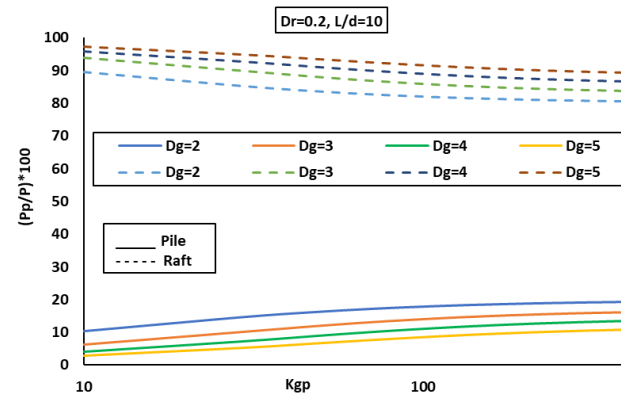


Figure 30: Variation of percentage load shared by GP ( $P_{gp}$ ) and Raft with  $K_{gp}$  – effect of annular width,  $D_g$ .

The shear stresses at the top and base of the GPs for different parameters are listed in Table 3. As per the results, increasing the annular ratio and annular width reduces the shear stresses significantly at the top and base of the

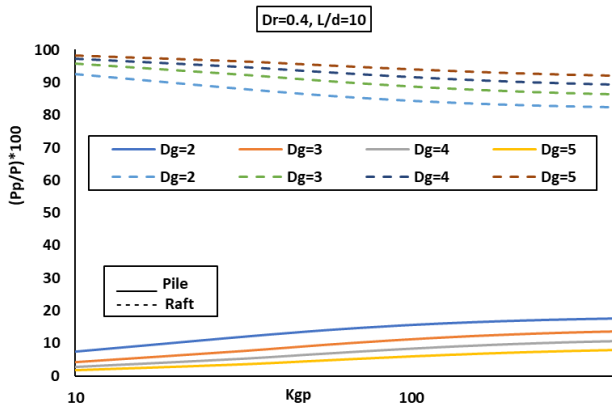


Figure 31: Variation of percentage load shared by GP ( $P_{gp}$ ) and raft with  $K_{gp}$  – effect of the annular width,  $D_g$ .

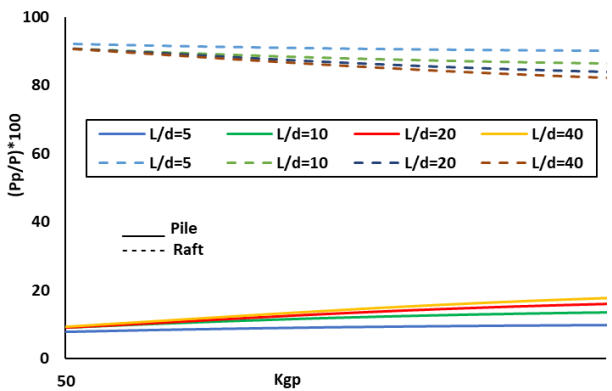


Figure 32: Variation of percentage load shared by GP ( $P_{gp}$ ) and raft with  $K_{gp}$  – effect of  $L/d$ .

GPs. The reduction in shear stress results from the wider annular width, which has more raft area to distribute the load and space between the GPs.

The effect of number of GPs on shear stress variation with normalized depth ( $Z_i$ ) is also evaluated and depicted in Figure 28. The shear stress variation is evaluated for  $D_r=0.4$  and  $D_g=3$ , and the effect of number of GPs is evaluated. It is observed that shear stresses  $\tau_1$  decreased with depth with the increase of no. of GPs due to a reduction in the load carried by GPs. The results indicate that as the number of granular piles increases, the shear stresses ( $\tau_i$ ) decrease with depth. This decrease can be attributed to the fact that an increased number of granular piles leads to a reduction in the load carried by each pile. Consequently, the load is more evenly distributed among a more significant number of piles, resulting in a decrease in shear stresses with increasing depth. This behavior can be attributed to the enhanced load-sharing capacity of the

granular piles, which leads to a more efficient distribution of loads within the system.

The variation of shear stresses normalized with load,  $P_p$ , carried by GPs,  $\tau_1^*$ , with the normalized depth is also evaluated and depicted in Figure 29. The normalized shear stresses  $\tau_1^*$  decrease over the top 75% length of the GPs but increase over the rest of their length.

The influence of annular width is analyzed and depicted in Figure 30 in the form of variation of the percentage of applied load carried by GP ( $P_p/P \times 100$ ) with  $K_{gp}$ . The percentage of load transferred to GPs increased from 10.41% for  $K_{gp}=10$  to 19.35% for  $K_{gp}=400$  for the annular raft with  $D_r=0.2$  and  $D_g=2$ , i.e., comparatively smaller annular raft. By increasing the annular width of the annular raft from 2 to 5, the percentage load transferred to GPs decreased as the raft size increased, and the raft is participating more as compared to GPs in load bearing due to the increased size of the annular raft. For  $D_g=5$ , the percentage of load transferred to GPs increased from 2.78% for  $K_{gp}=10$  to 10.80% for  $K_{gp}=400$ .

Similarly, the percentage load shared by GPs ( $P_{gp}$ ) is evaluated for a greater annular ratio, i.e.,  $D_r=0.4$ , and the effect of  $D_g$  is depicted in Figure 31. It is observed from the results that for the same annular width, i.e.,  $D_g=2$ , by increasing the annular ratio,  $D_r=0.2$  to 0.4, the percentage load shared by GPs decreased. For  $D_r=0.4$ , by increasing the annular width, the percentage load shared by GPs gets reduced, the same as seen in Figure 30. For  $D_r=0.4$ ,  $D_g=2$ , the percentage of load transferred to GPs increased from 7.48% for  $K_{gp}=10$  to 17.57% for  $K_{gp}=400$ . By increasing the annular width, i.e.,  $D_g=5$ , the percentage of load transferred to GPs increased from 1.78% for  $K_{gp}=10$  to 7.90% for  $K_{gp}=400$ .

The variation of percentage load shared by GPs ( $P_{gp}$ ) with  $K_{gp}$  for GPs of different  $L/d$  is depicted in Figure 32. It is observed from the results that by increasing  $K_{gp}$  of the GPs, the percentage load shared by GPs increases significantly. The improvement in the load shared by GPs is higher for GPs having greater  $L/d$ . It is also observed that the rate of load shared by GPs increases as the  $K_{gp}$  increases. By increasing the value of  $K_{gp}$  from 50 to 400, the load shared by the GP of  $L/d=40$  increased from 9.5% to 18%. The significant change in the load sharing of GPs is observed by increasing  $K_{gp}$  and  $L/d$  of GPs. As the parameter  $K_{gp}$  increases, there is a corresponding increase in the load-bearing capacity of the GP, leading to an escalation in the value of  $P_{gp}$ . Additionally, an observed trend indicates that  $P_{gp}$  increases with an augmentation in  $L/d$ , signifying that a GP having larger  $L/d$  is capable of carrying a greater load in comparison to a GP with a smaller  $L/d$ .

## 9 Conclusions

Analysis of an annular raft over four granular piles based on an elastic continuum approach is presented. The effects of various geometric and relative stiffness parameters on the response of the annular raft–GP system are quantified in terms of settlement influence factor, percentage load carried by the GPs, and the GP shaft–soil interface stresses and the contact pressures beneath the raft. The following conclusions are made on the basis of the present study:

- As the parameter  $K_{gp}$  undergoes an incremental increase, there is a noteworthy and statistically significant decrease observed in the parameter  $I_{agpr}$ . For a given set of conditions with  $D_g=2$ ,  $D_r=0.2$ , and  $L/d=10$ , the computed values of  $I_{agpr}$  corresponding to  $K_{gp}$  values of 10 and 400 are 0.127 and 0.085, respectively. This numerical comparison reveals a substantial decrease of 33.07% in the value of  $I_{agpr}$ , underscoring the pronounced impact of  $K_{gp}$  on the observed trend.
- The influence of the parameter  $K_{gp}$  on the values of  $I_{agpr}$  is discerned across varying levels of  $D_r$ . Specifically, at  $K_{gp}=10$ , the computed values of  $I_{agpr}$  for  $D_r=0.2, 0.4, 0.6$ , and  $0.8$  are 0.127, 0.103, 0.075, and 0.041, respectively, for a given set of conditions with  $L/d=10$  and  $D_g=2$ . Notably, the analysis reveals that as  $D_r$  increases, there is an escalated percentage decrease in  $I_{agpr}$  by 18.89%, 40.94%, and 67.71% for  $D_r=0.4, 0.6$ , and  $0.8$ , respectively, relative to the reference value of  $I_{agpr}$  at  $D_r=0.2$ , which is 0.127.
- The parameter  $L/d$  exerts a pronounced influence on the values of  $I_{agpr}$ . Given a set of conditions with  $D_g=2$ ,  $D_r=0.4$ , and  $K_{gp}=400$ , the computed values of  $I_{agpr}$  exhibit a noticeable trend: 0.094, 0.074, 0.056, and 0.043 for  $L/d$  ratios of 5, 10, 20, and 40, respectively. The observed pattern reveals a significant decrease in  $I_{agpr}$  with increasing  $L/d$  ratios, resulting in percentage reductions of 21.27%, 40.42%, and 54.25% concerning the baseline  $I_{agpr}$  value at  $L/d=5$ , which is 0.094. These outcomes underscore a substantial decrease in  $I_{agpr}$  associated with a larger granular pile, indicating a noteworthy structural response to varying length-to-diameter ratios.
- The shear stresses at the top exhibit lower values in comparison to the base, primarily attributed to the induced shear stresses with increasing depth. Notably, an observation revealed a significant percentage increase of 226.9% in shear stresses from the top to the bottom for conditions characterized by  $D_r=0.2$ ,  $K_{gp}=100$ ,  $D_g=2$ , and  $L/d=10$ . However, it is noteworthy that an increase in  $D_g$  leads to a reduction in shear stresses compared to the reference case of  $D_g=2$ . This

phenomenon can be attributed to the increased annular width, resulting in a larger raft area, which, in turn, diminishes the load transfer to the piles.

- The percentage load carried by GP increases with the increase of its stiffness and decreases with the increase of the relative size of raft. The raft–soil interface normal stresses decrease with the increase of stiffness of GP. The influences of GP stiffness and relative length of GP are found to be more for relatively large size of raft. A significant change in the GP behavior due to the presence of the raft is to transfer the load to points at depth, i.e., the percentage of load transferred to the base of GP increases with the increase of the relative size of the raft.
- The settlement influence factor for the annular raft decreases with the increase of the annular ratio, the annular width, and the stiffness of GP. For a higher annular ratio or annular width, i.e., the influence of granular piles on the settlement reduction of an annular raft is limited. The ratio of settlement of annular raft depends on the same parameters as stated above. The percentage load transferred to GP increases with the increase of stiffness of GP and/or relative length of GP, while it decreases with the increase of annular ratio and annular width.

**Acknowledgment:** The first author is highly grateful to the late Dr. Vaibhaw Garg for his valuable discussion. His positive attitude played a significant role in writing this research.

## References

- [1] Randolph, M. F., & Wroth, C. P. (1978). Analysis of deformation of vertically loaded piles. *Journal of the geotechnical engineering division*, 104(12), 1465-1488.
- [2] Poulos, H. G., & Davis, E. H. (1980). *Pile foundation analysis and design* (Vol. 397). New York: Wiley.
- [3] O'Neill, M. W., & Raines, R. D. (1991). Load transfer for pipe piles in highly pressured dense sand. *Journal of Geotechnical Engineering*, 117(8), 1208-1226.
- [4] Madhav, M.R. 1982. Recent developments in the analysis and design of granular piles. *Symp. On Soil and Rock Improvement Tech.* Bangkok, Thailand, Dec, 117-129.
- [5] Van Impe, W.F. and De Beer, E. 1983. Improvement of settlement behavior of soft layers by means of stone columns. *Proc.7<sup>th</sup> ECSMFE, Helsinki*, Vol. 1, pp. 1207-1210.
- [6] Madhav, M. R. and, Van Impe, W.F. 1994. Load transfer through a gravel bed on stone column reinforced soil. *Geotechnical Engineering*, Vol. 24, No.2, 47-62.

- [7] Madhav M. R. and Nagpure, D.D. 1995. Granular piles- a low-cost alternative to R.C.C piles. Seminar on Ground Improvement Techniques, GRIMTECH, Indore, pp. 17-29.
- [8] Sharma, J.K. 1999. Analysis and settlement of granular pile(s) – single, in group and with raft. *A Ph. D. Dissertation submitted to Department of Civil Engineering, Indian Institute of Technology, Kanpur.*
- [9] Sharma, J.K. and Gupta, P. (2018) “Consideration of Nonlinear Non-homogeneity of Floating Granular Pile and Soil on Settlement”, *Journal of The Institution of Engineers (India)*, 1-11, series A
- [10] Hasan, M., & Samadhiya, N. K. (2017). Performance of geosynthetic-reinforced granular piles in soft clays: model tests and numerical analysis. *Computers and Geotechnics*, 87, 178-187.
- [11] Hasan, M., & Samadhiya, N. K. (2022). Ground Improvement by Using Floating Granular Piles: Experimental Studies and Numerical Investigations. In *Earthquake Geotechnics: Select Proceedings of 7th ICORAGEE 2021* (pp. 465-475). Springer Singapore.
- [12] Poulos, H.G., 2001. Piled raft foundations: design and applications. *Geotechnique*, 51(2), pp.95-113. doi:10.1680/geot.51.2.95.40292.
- [13] Balaam, N.P., Poulos, H.G. and Brown, P.T. 1977. Settlement analysis of soft clays reinforced with granular piles. *Proc.5<sup>th</sup> ARC, Bangkok, Thailand, Vol. 1*, pp. 8192.
- [14] Madhav, M. R., Sharma, J. K. and Sivakumar, V. 2009. Settlement of and load distribution in a granular piled raft, *Geomechanics and engineering Journal*, Vol.1, (1), 97–112.
- [15] Kumar, A., D. Choudhury, and R. Katzenbach. 2016. “Effect of Earthquake on Combined Pile–raft Foundation.” *International Journal of Geomechanics* 16 (5): 04016013. doi:10.1061/(ASCE)GM.1943-5622.0000637.
- [16] Sinha, A., and A. Hanna. 2016. “3D Numerical Model for Piled Raft Foundation.” *International Journal of Geomechanics* 17 (2): 04016055. doi:10.1061/(ASCE)GM.1943-5622.0000674.
- [17] Samanta, M., & Bhowmik, R. (2017). 3D numerical analysis of piled raft foundation in stone column improved soft soil. *International Journal of Geotechnical Engineering*.
- [18] Deb, P., & Pal, S. K. (2022). Structural and geotechnical aspects of piled raft foundation through numerical analysis. *Marine Georesources & Geotechnology*, 40(7), 823-846.
- [19] Roy, J., A. Kumar, and D. Choudhury. 2018. “Natural Frequencies of Piled Raft Foundation Including Superstructure Effect.” *Soil Dynamics and Earthquake Engineering* 112: 69–75. doi:10.1016/j.soildyn.2018.04.048.
- [20] Roy, J., A. Kumar, and D. Choudhury. 2020. “Pseudostatic Approach to Analyze Combined Pile-raft Foundation.” *International Journal of Geomechanics* 20 (10): 06020028. doi:10.1061/(ASCE)GM.1943-5622.0001806.
- [21] Clancy P, Randolph MF (1993) An approximate analysis procedure for piled raft foundations. *Int J Numer Anal Meth Geomech* 17(12):849-869. <https://doi.org/10.1002/nag.1610171203>
- [22] Bandyopadhyay, S., Sengupta, A., & Parulekar, Y. M. (2020). Behavior of a combined piled raft foundation in a multi-layered soil subjected to vertical loading. *Geomech. Eng*, 21(4), 379-390.
- [23] Mandolini, A., Di Laora, R., & Mascarucci, Y. (2013). Rational design of piled raft. *Procedia Engineering*, 57, 45-52.
- [24] Solanki, A., Sharma, J. K., & Madhav, M. R. (2022). Interaction analysis of two floating granular piled raft units. *Geomechanics and Geoengineering*, 1-18.
- [25] Ornek, M., Laman, M., Demir, A. and Yildiz, A., 2012. Prediction of bearing capacity of circular footings on soft clay stabilized with granular soil. *Soils and Foundations*, 52(1), pp.69-80.
- [26] Sargazi, O. and Hosseininia, E.S., 2017. Bearing capacity of ring footings on cohesionless soil under eccentric load. *Computers and Geotechnics*, 92, pp.169-178.
- [27] Al-Azzawi, A.A. and Daud, K.A., 2019, August. Numerical analysis of thin ring foundations under different loading conditions. In *IOP Conference Series: Materials Science and Engineering* (Vol. 584, No. 1, p. 012050). IOP Publishing.
- [28] Xiao, Y., Zhao, M., Zhao, H. and Zhang, R., 2020. Numerical study on bearing capacity of ring foundations for storage tanks on a rock mass. *Arabian Journal of Geosciences*, 13(23), pp.1-9.
- [29] Prasad, S.D. and Chakraborty, M., 2021. Bearing capacity of ring footing resting on two layered soilsoils. *Computers and Geotechnics*, 134, p.104088.
- [30] Das, P.P., Khatri, V.N. and Dutta, R.K., 2021. Bearing capacity of ring footing on weak sand layer overlying a dense sand deposit. *Geomechanics and Geoengineering*, 16(4), pp.249-262.
- [31] Birid, K. and Choudhury, D., 2021. Undrained bearing capacity factor  $N_c$  for ring foundations in cohesive soil. *International Journal of Geomechanics*, 21(2), p.06020038.
- [32] Birid, K. and Choudhury, D., 2021. Undrained bearing capacity factor  $N_c$  for ring foundations in cohesive soil. *International Journal of Geomechanics*, 21(2), p.06020038.
- [33] Yodsomjai, W., Keawsawasvong, S. and Lai, V.Q., 2021. Limit analysis solutions for bearing capacity of ring foundations on rocks using Hoek–Brown failure criterion. *International Journal of Geosynthetics and Ground Engineering*, 7(2), pp.1-10.
- [34] Birid, K. and Choudhury, D., 2022. Bearing capacity of ring foundations over a rock mass using numerical analysis. *Geomechanics and Geoengineering*, 17(6), pp.2013-2039.
- [35] Becker, D.E. and Lo, K.Y., 1979. Settlement and load transfer of ring foundation for tower silos. *Canadian agricultural engineering*, 21(2), pp.97-110.
- [36] Das, B. and Sivakugan, N., 2007. Settlements of shallow foundations on granular soil—an overview. *International journal of geotechnical engineering*, 1(1), pp.19-29.
- [37] Naseri, M. and Hosseininia, E.S., 2015. Elastic settlement of ring foundations. *Soils and Foundations*, 55(2), pp.284-295.
- [38] Lee, J.K. and Jeong, S., 2018. Immediate settlement of ring footings resting on inhomogeneous finite stratum. *Applied Sciences*, 8(2), p.255.
- [39] Taghavi Ghalesari, A. and Janalizadeh Choobbasti, A., 2018. Numerical analysis of settlement and bearing behaviour of piled raft in Babol clay. *European Journal of Environmental and Civil Engineering*, 22(8), pp.978-1003.
- [40] Shiuly, A. and Roy, S., 2021. Study on Settlement Behaviour of Annular Raft Foundation using Finite Element–Boundary Element Method. *Iranian Journal of Science and Technology, Transactions of Civil Engineering*, 45(3), pp.1705-1721.
- [41] Zhang, J. and Du, R., 2021, July. Study on calculation and analysis of foundation settlement in cooling tower. In *IOP Conference Series: Earth and Environmental Science* (Vol. 804, No. 2, p. 022009). IOP Publishing.

- [42] Rathor, A.P.S., Sharma, J.K., 2022. Numerical Evaluation of Settlement and Stresses of Annular Raft. *J. Inst. Eng. India Ser. A* (2022). doi:10.1007/s40030-022-00707-4
- [43] Sharma, J. K., & Sanadhya, R. R. (2022). Analysis of rigid raft overlying the granular pile with the effect of stiffness of bearing stratum. *Geomechanics and Geoengineering*, 17(1), 166-187.
- [44] Madhav, M. R., Sharma, J. K., & Chandra, S. (2006). Analysis and settlement of a non-homogeneous granular pile. *Indian Geotechnical Journal*, 36(3), 249-271.
- [45] Mindlin, R.D. 1936. Force at a point in the interior of a semi-infinite solid. *Physics*, 7, 195–202. doi:10.1063/1.1745385
- [46] Mindlin, R.D., 1937. Stress system in a circular disk under radial forces, presented at the joint meeting of applied mechanics and hydraulic division of the ASME held at Cornell University, NY, 115–118. 10.1115/1.4008786.
- [47] Boussinesq, J., 1885. Application of potentials to the study of the equilibrium and motion of elastic solids: mainly to the calculation of the strains and pressures produced, in these solids, by any forces exerted on a small part of their surface or of their interior: thesis followed by extensive notes on various points of physics, mathematics and analysis. Vol. 4. Gauthier-Villars, Paris, pp. 30.
- [48] Garg, V., & Sharma, J. K. (2020). Analyses and settlement study of a group of two, three and four partially stiffened floating granular piles. *Geomechanics and Geoengineering*, 15(3), 203-223.
- [49] Al-Sanad, H.A., Ismael, N.F. and Brenner, R.P., 1993. Settlement of circular and ring plates in very dense calcareous sands. *Journal of geotechnical engineering*, 119(4), pp.622-638.
- [50] Egorov, K.E. (1965). "Calculation of bed for foundation with ring footing." *Proc., 6<sup>th</sup> Int. Conf. Soil Mech. And Found. Engrg., Montreal*, 2, 41-45.